

Effect of the large-scale atmospheric circulation on the variability of the Arctic Ocean freshwater export

Alexandra Jahn · Bruno Tremblay · Lawrence A. Mysak · Robert Newton

Received: 14 July 2008 / Accepted: 14 March 2009

Abstract Freshwater (FW) leaves the Arctic Ocean through sea-ice export and the outflow of low-salinity upper ocean water. Whereas the variability of the sea-ice export is known to be mainly caused by changes in the local wind and the thickness of the exported sea ice, the mechanisms that regulate the variability of the liquid FW export are still under investigation. To better understand these mechanisms, we present an analysis of the variability of the liquid FW export from the Arctic Ocean for the period 1950–2007, using a simulation from an energy and mass conserving global ocean-sea ice model, coupled to an Energy Moisture Balance Model of the atmosphere, and forced with daily winds from the NCEP reanalysis. Our results show that the simulated liquid FW exports through the Canadian Arctic Archipelago (CAA) and the Fram Strait lag changes in the large-scale atmospheric circulation over the Arctic by 1 and 6 years, respectively. The variability of the liquid FW exports is caused by changes in the cyclonicity of the atmospheric forcing, which cause a FW redistribution in the Arctic through changes in Ekman transport in the Beaufort Gyre. This in turn causes changes in the sea surface height (SSH) and salinity upstream of the CAA and Fram Strait, which affect the velocity and salinity of the outflow. The SSH changes induced by the large-scale atmospheric circulation are found to explain a large part of the variance of the liquid FW export, while the local wind plays a much smaller role. We also show that during periods of increased liquid FW export from the Arctic, the strength of the simulated Atlantic meridional overturning circulation

(MOC) is reduced and the ocean heat transport into the Arctic is increased. These results are particularly relevant in the context of global warming, as climate simulations predict an increase in the liquid FW export from the Arctic during the 21st century.

Keywords Arctic Ocean · freshwater · modeling · MOC · ocean heat flux

1 Introduction

The upper Arctic Ocean contains a large amount of freshwater (FW) relative to the mean Arctic salinity of 34.8 (e.g., Aagaard and Carmack, 1989; Serreze et al, 2006). A part of this FW is drained from the Arctic Ocean through the export of sea ice and low-salinity upper ocean water through Fram Strait and the Canadian Arctic Archipelago (CAA). This FW transport is important because it influences the stratification of the water column in the sensitive deep water formation regions of the Greenland, Icelandic, Norwegian (GIN), and Labrador seas. Hence, changes in the FW export from the Arctic can affect the strength of the Atlantic meridional overturning circulation (MOC) (e.g., Aagaard et al, 1985; Aagaard and Carmack, 1989; Weaver et al, 1993; Häkkinen, 1995; Lohmann and Gerdes, 1998; Holland et al, 2001). Moreover, changes in the sea-ice cover of the Arctic Ocean can affect the local thermohaline circulation due to a positive feedback between sea-ice melt, increased sea-ice growth in areas of thin ice the following winter, and ocean heat fluxes in the Arctic. In fact, model simulations have shown that the density-driven oceanic heat transport from the GIN seas to the Arctic Ocean increases when the sea-ice cover decreases (Bitz et al, 2006).

In the classical climatological Arctic FW budget of Aagaard and Carmack (1989), the dominant source of FW for the GIN seas is sea-ice export, whereas liquid FW export

A. Jahn · L. A. Mysak · B. Tremblay
Department of Atmospheric and Oceanic Sciences, McGill University,
805 Sherbrooke Street West, Montréal, Québec, H3A 2K6, Canada
E-mail: ajahn@meteo.mcgill.ca

R. Newton · B. Tremblay
Lamont-Doherty Earth Observatory, Columbia University of New
York, Palisades, NY, USA

was estimated to contribute only one-third of the FW export due to sea ice (see Table 1). Most subsequent numerical studies have therefore focused on the interannual variability of the Fram Strait sea-ice export and its link to atmospheric variability (e.g., Häkkinen, 1995; Proshutinsky and Johnson, 1997; Harder et al, 1998; Mysak and Venegas, 1998; Vinje et al, 1998; Kwok and Rothrock, 1999; Arfeuille et al, 2000; Dickson et al, 2000; Hilmer and Jung, 2000; Tremblay, 2001; Vinje, 2001; Kauker et al, 2003). However, measurements of the meteoric water flow (which only accounts for the diluting effect of the runoff and precipitation, and not for the salinification of the water due to sea-ice formation) through Fram Strait in August and September of 1997 and 1998 by Meredith et al (2001) found this flow to be about twice as large as the long-term mean FW export due to sea ice. Based on these new measurements, and taking into account the seasonal cycle of the velocity field in Fram Strait (Fahrbach et al, 2001), Serreze et al (2006) estimated that the liquid FW export through Fram Strait is about as large as the long-term mean of the Fram Strait sea-ice export (see Table 1). In addition, recent measurements by Prinsenbergh and Hamilton (2005) showed that the liquid FW export through the CAA is also at least twice as large as earlier measurements suggested, which makes it the largest liquid FW sink for the Arctic Ocean.

Compared to studies on the variability of the sea-ice export, there have been relatively few studies on the variability of the liquid FW export from the Arctic, and the mechanisms that control this variability remain under debate. Using rotating tank experiments, Hunkins and Whitehead (1992) showed that the general anticyclonic wind stress curl over the Arctic Ocean causes FW from the shelves to accumulate in the Beaufort Gyre region, which explains the high concentration of FW from Eurasian sources over the Canadian Basin. Furthermore, they demonstrated that changes in the gradient of the wind stress curl between the Arctic Ocean and the northern North Atlantic could modulate the oceanic exchange through Fram Strait. Based on model experiments, Proshutinsky et al (2002) suggested that the liquid FW content of the Beaufort Gyre changes between anticyclonic and cyclonic circulation regimes on a decadal timescale, due to Ekman convergence and divergence, respectively. Recent results from observations in the Beaufort Gyre support this model-based hypothesis (Proshutinsky et al, 2009). Results of Proshutinsky et al (2002) also suggest that the release of FW from the Beaufort Gyre during the cyclonic circulation regime is the most important factor for large changes in the liquid FW export. This agrees with results of Zhang et al (2003), who showed that under idealized positive Arctic Oscillation (AO) forcing, the Beaufort Gyre is weakened and the liquid FW export from the Arctic is increased by 12% compared to a simulation with idealized negative AO forcing. Using a simple analytical model of the Arctic Ocean to

investigate the response of the Arctic Ocean circulation to the annular mode, Newton et al (2006) also found that Ekman transport is important for the redistribution of FW in the Arctic. In their model, Ekman transport influenced the variability of the FW export from the Arctic through its effect on the pycnocline depth. Using numerical simulations from a regional ocean-sea ice model, Karcher et al (2005) showed that the negative salinity anomaly in the GIN seas in the 1990s was caused mainly by a large liquid FW export from the Arctic, in contrast to the sea-ice export dominated Great Salinity Anomaly of the late 1960s and early 1970s (e.g., Dickson et al, 1988; Mysak et al, 1990). They found that the large simulated liquid FW export in the mid 1990s was due to the export of much fresher water than usual, which was supplied by a large-scale redistribution of FW in the Arctic Ocean in response to the high positive phase of the North Atlantic Oscillation (NAO) during the period 1989–1995. In contrast, Häkkinen and Proshutinsky (2004) found that in their simulation the redistribution of FW in the Arctic Ocean due to Ekman transport had no significant impact on changes of the Arctic Ocean FW content. Instead changes in the Arctic FW content occur as result of barotropic transport anomalies in the exchange between the Arctic Ocean and the GIN seas in their model. Results by Köberle and Gerdes (2007) agree with this hypothesis. In their simulation changes in the Arctic FW distribution did not have an influence on the salinity of the outflow through Fram Strait after 1975.

There is no long-term observational record of the liquid FW export through Fram Strait or the CAA that could be used to constrain model simulations. As a result, no broad consensus on the mechanisms behind the variability of the liquid FW export has been reached. Given that model simulations for the 21st century show an increase in the liquid FW export from the Arctic Ocean and a decrease in the sea-ice export (e.g., Haak et al, 2005; Holland et al, 2006, 2007; Koenigk et al, 2007), a better understanding of the mechanisms that govern the variability of the liquid FW export and the associated ocean heat transport is clearly important. This is the focus of the present article.

In the following, we investigate the interannual variability of the Arctic FW budget, focussing on the mechanisms that control changes in the liquid FW export from the Arctic Ocean, as well as on the effect that changes in the liquid FW export have on the poleward oceanic heat flux and the Atlantic MOC. In contrast to previous model studies, which used regional coupled ocean-sea ice models (e.g., Proshutinsky et al, 2002; Häkkinen and Proshutinsky, 2004; Karcher et al, 2005; Newton et al, 2006; Köberle and Gerdes, 2007), we use a global ocean-sea ice model coupled to an Energy Moisture Balance Model (EMBM) of the atmosphere, namely the University of Victoria Earth System Climate Model (UVic ESCM). We show that in this

model it is the variability of the large-scale atmospheric circulation that controls the variability of the liquid FW export from the Arctic through its effect on the strength and location of the Beaufort Gyre. The CAA liquid FW export is found to respond to changes in the atmospheric forcing with a lag of 1 year, whereas the mean lag of the Fram Strait liquid FW export is 6 years.

The article is structured as follows: In section 2 we describe the model and the model simulations. A brief overview of the performance of the model in the Arctic is given in section 3. In section 4 the simulated Arctic Ocean FW budget is presented, and in section 5 we discuss the mechanisms that control the variability of the liquid FW export through the CAA and Fram Strait, and compare our results to previous work. In section 6 we examine the effects of the liquid FW export on the oceanic heat flux into the Arctic Ocean and on the Atlantic MOC. Finally, the main conclusions from this study are summarized in section 7.

2 Model

2.1 Model description

The UVic ESCM is a global ocean-sea ice model coupled to an EMBM for the atmosphere that was developed at the University of Victoria (Weaver et al, 2001). It does not use salinity or temperature restoring, and conserves energy and salt to machine precision. Since its release, the UVic ESCM has been successfully used to study many different processes in the Arctic Ocean and the North Atlantic region (e.g., Holland et al, 2001; Saenko et al, 2003; Gregory et al, 2003; Saenko et al, 2004; Mysak et al, 2005; Rennermalm et al, 2006, 2007; Sedláček et al, 2007; Sedláček and Mysak, 2009). Here we use the most recent version of the UVic ESCM (version 2.8).

The ocean component of the UVic ESCM is the Geophysical Fluid Dynamics Laboratory Modular Ocean Model (MOM) (Pacanowski, 1995), version 2.2. It is a rigid-lid model and uses a second-order centered difference advection scheme for momentum advection. Constant horizontal and vertical mixing coefficients are used for the mixing of momentum. The flux-corrected transport (FCT) algorithm is used for tracer advection. For the mixing of tracers, isopycnal mixing and the parametrization of mesoscale eddy-induced mixing by Gent and McWilliams (1990) are used. The combination of the FCT advection scheme with the Gent-McWilliams parametrization has been shown to improve the simulation of tracer distributions over the use of Laplacian or biharmonic horizontal/vertical diffusion (Weaver and Eby, 1997). Surface FW fluxes are added to the ocean as a negative salt flux by multiplying the volume flux with a fixed global surface reference salinity of 34.84. The sea-ice model thermodynamics are based on

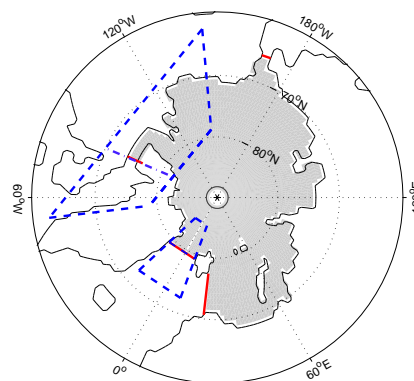


Fig. 1 Definition of the Arctic Ocean domain used in the FW budget calculations (shaded in grey); it is the same as in Serreze et al (2006). The ocean boundaries where inflows and outflows are calculated are shown in red (Bering Strait, Fram Strait, Canadian Arctic Archipelago (CAA), and Barents Sea). The coastline of the UVic ESCM is shown as a black line. The dashed blue lines show the regions used to calculate sea surface height differences for the Fram Strait and CAA (see section 5).

the energy-conserving algorithm of Bitz et al (2001), and the model uses a zero-layer thermodynamic scheme with two categories (sea ice and open water). The dynamics are based on the elastic-viscous-plastic sea-ice model of Hunke and Dukowicz (1997).

The atmospheric component of the UVic ESCM is an EMBM that is loosely based on the model of Fanning and Weaver (1996). It is forced by prescribed NCEP wind forcing (Kalnay et al, 1996), and heat and moisture are transported by advection. The EMBM is coupled to the ocean model every 2.5 days using a leapfrog scheme. Due to different east-west and north-south diffusion coefficients in this most recent version of the EMBM, the current version of the UVic ESCM can not be used with a rotated coordinate system, and therefore has an artificial island at the North Pole. However, simulations with different sizes of the island, as well as with an earlier version of the model that could be used with a rotated grid, showed that the North Pole island does not change the conclusions presented in this paper.

2.2 Model simulations

The standard resolution of the UVic ESCM is 3.6° zonally and 1.8° meridionally, with 15 vertical levels. In this study we use a higher resolution version with a grid spacing of 1.8° zonally and 0.9° meridionally, with 32 unequally spaced levels in the ocean (ranging from a thickness of 50 m at the surface to 298 m at the bottom). As an improvement over the lower resolution model, this higher resolution version allows for the water exchange between the Pacific and the Arctic oceans through Bering Strait and between

the Arctic Ocean and the Labrador Sea through one channel representing the CAA. The higher resolution also allows for a better resolution of ocean currents between the Arctic Ocean and the GIN Seas.

Since any channel in the model must be at least two grid boxes deep and wide, the Bering Strait opening in the model is 108 m deep and 225 km wide, compared with an observed depth and width of 50 m and 85 km, respectively. To reduce the mass exchange through the channel, the bottom drag in Bering Strait was increased, following the approach of Andreas Schmittner (personal communication, 2006). This modification reduced the volume flux through Bering Strait from 2.7 Sv to 1.2 Sv, which is in much better agreement with the observed volume flow of about 1 Sv (Woodgate and Aagaard, 2005). It also reduced the inflow of water in the second layer of the ocean model (between 50 m and 108 m) from 1.2 Sv to 0.2 Sv, which is important as it affects the total FW flux through Bering Strait, as well as the depth at which the FW is delivered to the Arctic Ocean. The CAA is represented in the model as one channel, which is 200 km wide and 330 m deep. The simulated annual mean volume flux through this channel is 1.5 Sv, which is within the range of the observational estimates of 1.5–2 Sv for the total volume flux through the CAA (Prinsenbergh and Hamilton, 2005).

Precipitation in the high latitudes is underestimated in the UVic ESCM, which leads to a simulated river runoff into the Arctic Ocean that is approximately half of the observed runoff. Following Rennermalm et al (2006), we specify the monthly climatological river discharge data for all rivers draining into the Arctic Ocean, using data from R-Arctic Net version 2 (Lammers et al, 2001). The model still conserves energy and mass by using a very small (< -8 mm/year) and nearly time invariant ($\text{std} < 0.3$ mm/year) surface salinity flux to make up for the difference between modeled and prescribed river runoff. By using the discharge climatology, the interannual variability in the runoff is eliminated. However, observations show that the river runoff variability is small compared with the variability of the Bering Strait FW inflow and the FW export by sea-ice (Serreze et al, 2006). To study the variability of the FW budget, this approach is preferred over the use of salinity restoring, as it does not introduce an unrealistic salinity feedback.

The UVic ESCM was initialized with temperature and salinity data from the World Ocean Atlas 2001. It was then integrated for 200 years, forced with pre-industrial (i.e., 1850) atmospheric CO_2 conditions and solar insolation values at the top of the atmosphere, prescribed climatological river discharge, and random years of daily varying NCEP winds (Kalnay et al, 1996). In a second spin-up, the model was run for the period 1850–1947, forced with temporally varying solar insolation and atmospheric CO_2 concentration, as well as with random years of daily varying

NCEP winds and prescribed climatological river discharge. Finally, the simulation used in this study was forced with 1948–2007 daily varying NCEP winds, which were read in every 2.5 days (the coupling time between the atmosphere and ocean model). Atmospheric CO_2 concentrations and solar insolation values were set in accordance with Keeling and Whorf (2005) and Berger (1978), respectively. For the river runoff, climatological discharge was prescribed throughout. The diagnostic model output was written every 2.5 days. In the following, we analyze the model output from 1950 to 2007, neglecting the first two years of the simulation during which the effect of the random initial conditions is strongest (see section 4.4).

The Arctic Ocean domain used for the FW budget calculation is shown in Fig. 1. Oceanic FW fluxes are calculated offline from the model output for Bering Strait, the CAA, Fram Strait, and the passage between Svalbard and Norway along 23.4° E (referred to as Barents Sea fluxes hereafter). Influxes into the Arctic Ocean were defined positive, outflows negative. The reference salinity used to calculate the FW budget of the Arctic Ocean in this study is 34.8, which is the average salinity of the Arctic Ocean (Aagaard and Carmack, 1989).

3 Simulated Arctic Ocean conditions

The mean simulated total (solid plus liquid) FW content in the upper 518 m of the Arctic Ocean is $103,789 \text{ km}^3$ relative to the reference salinity of 34.8, with $96,474 \text{ km}^3$ stored as liquid FW (negative FW allowed) and $7,315 \text{ km}^3$ stored as solid FW in the Arctic sea-ice cover. Compared to the estimates of Serreze et al (2006) based on the PHC data of Steele et al (2001), the simulated liquid FW storage in the Arctic Ocean is larger ($96,474 \text{ km}^3$ in the model versus $74,000 \pm 7400 \text{ km}^3$), while the solid FW storage in the Arctic sea-ice cover is smaller ($7,315 \text{ km}^3$ in the model versus $10,000 \text{ km}^3$). As shown in Fig. 2, the simulated mixed layer in the central Arctic Ocean is characterized by saltier and colder than observed water, with fresher than observed water beneath the mixed layer down to about 500 m. As a consequence of this density structure, the core of the warm and salty Atlantic water in the central Arctic Ocean is located lower than in the PHC data (700 m versus 400 m), and the simulated 34.8 salinity surface is found at around 500 m instead of between 200–300 m. Atlantic water also does not penetrate the Arctic Ocean as much as observed and is colder (see Fig. 2).

The simulated spatial distribution of the FW storage in the Arctic Ocean shows similar features to the observed distribution (see Fig. 3), but also some differences. The simulated FW storage in the Beaufort Gyre is smaller than observed, and shows a slightly different shape than the PHC

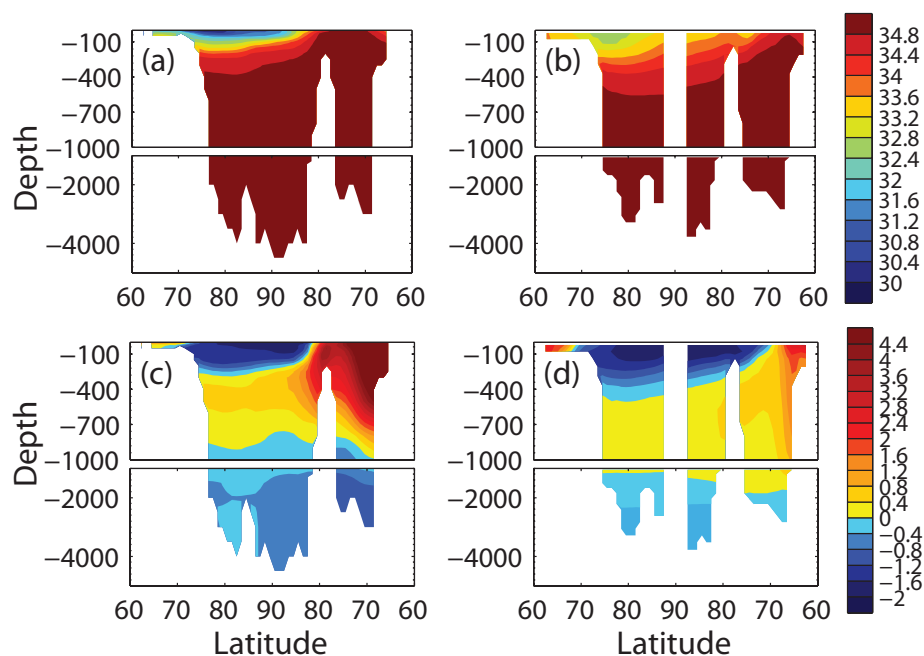


Fig. 2 Salinity (a–b) and temperature (c–d) [$^{\circ}\text{C}$] cross sections through the Arctic Ocean from Bering Strait (*left side of panel*) to Fram Strait (*right side of panel*) along longitude 10°E and 10°W . Results from the updated PHC data of Steele et al (2001) are shown in (a) and (c), model results in (b) and (d).

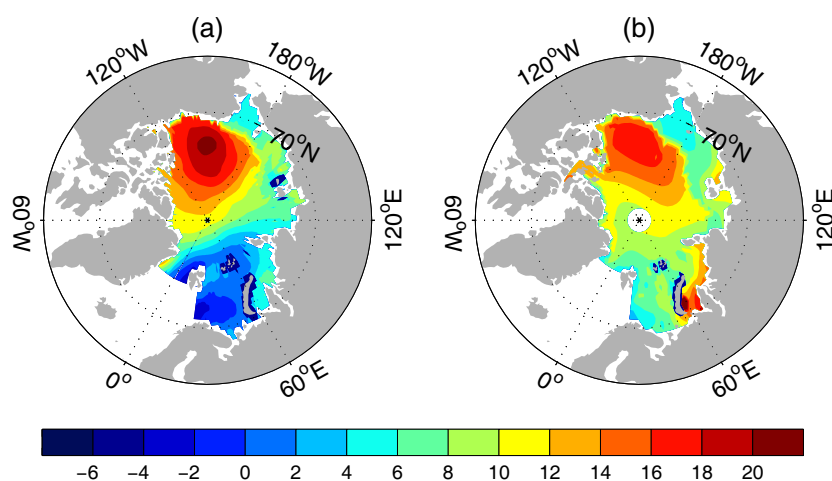


Fig. 3 Liquid FW content, expressed as the thickness of the FW column in the upper 500 m of the water column [m], from (a) the updated PHC data of Steele et al (2001) and (b) the model simulation, averaged over 1950–2007. Negative FW in the figures shows regions where the water column is fresher than the reference salinity of 34.8.

data. Larger than observed FW storage is seen in the Barents and Kara seas, due to the too small transport of Atlantic water into the Barents Sea. The different shape of the FW storage in the Beaufort Sea could be due to a bias in the NCEP wind forcing, as a model simulation of Köberle and Gerdes (2007), forced by the same winds, shows a very similar pattern as seen here.

The simulated Arctic sea-ice cover is too thin (see Fig. 4), which leads to the smaller than observed simulated solid FW storage ($7,315 \text{ km}^3$). Due to sparse sea-ice

thickness data, the observational estimates of the solid FW storage range between $10,000 \text{ km}^3$ (Serreze et al, 2006) and about $16,000 \text{ km}^3$ (Aagaard and Carmack, 1989), depending mainly on whether an average annual sea-ice thickness of 2 m or 3 m is used in the estimates. Even though the sea-ice thickness is generally too small, the relative spatial distribution of the ice thickness and relative changes between winter and summer ice thickness and cover compare well with the AOMIP and IPCC models shown in Gerdes and Köberle (2007). As shown in Fig. 4b,

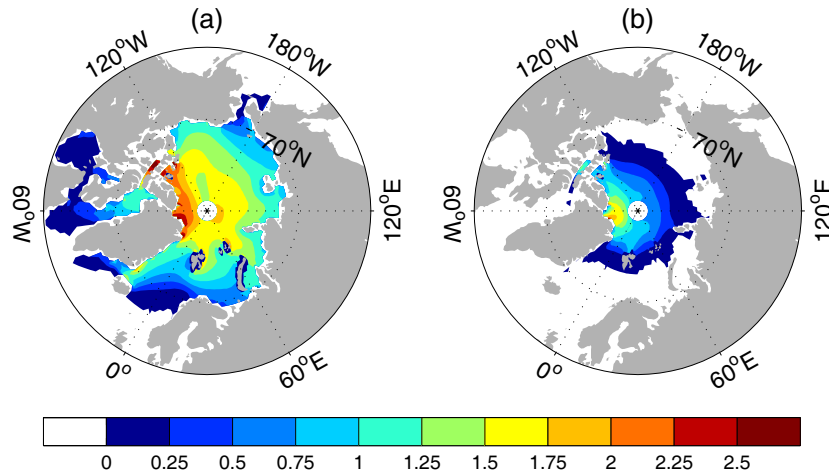


Fig. 4 Mean (1950–2007) simulated sea ice thickness [m] in (a) April and (b) September.

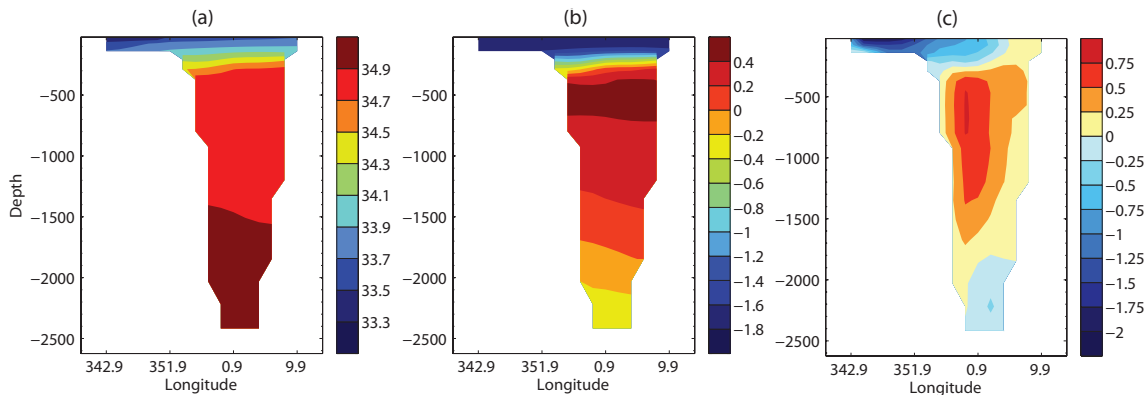


Fig. 5 Simulated (a) salinity, (b) temperature [$^{\circ}\text{C}$], and (c) velocity [cm/s] in a west-east cross section through Fram Strait (along 79.2°N), which shows the currents of Atlantic and Arctic water in Fram Strait. The velocity field shown is perpendicular to the cross section area, and negative velocities mean a southward transport.

the Barents, Kara, Laptev, and Siberian seas are ice-free in September, and the thickest sea ice is found north of Greenland (Fig. 4). However, the relative thickness of the sea ice in the Beaufort Sea is too small compared to many of the AOMIP models, and the winter sea-ice edge is located too far south compared to other models and observations.

The too extensive sea-ice cover in the Barents Sea leads to a simulated sea-ice export out of the Barents Sea that is not observed. This is a common problem of relatively coarse resolution global ocean models, and is related to the underestimated ocean heat transport from the North Atlantic Drift into the Arctic Ocean (Weaver et al, 2001). Reducing the model resolution from the standard $3.6^{\circ} \times 1.8^{\circ}$ resolution of the UVic ESCM to $1.8^{\circ} \times 0.9^{\circ}$ improved the simulated sea-ice edge and decreased the sea-ice export through Barents Sea by 30%, but the sea ice still extends too far south compared to observations. This leads to a stratified upper ocean in the GIN seas in the model, with the North Atlantic Drift entering the Arctic Ocean at depth (below 330 m) instead of

at the surface (see Fig. 5), a feature also seen in many other models (e.g. Prange and Gerdes, 2006; Komuro and Hasumi, 2005; Zhang et al, 1998; Häkkinen and Mellor, 1992). The export of Arctic surface water occurs in the upper 330 m of Fram Strait in the model (Fig. 5), with higher velocities in the East Greenland Current during winter than during summer (Fig. 6). The model also captures the observed inter-annual changes in the strength of the Beaufort Gyre, with a more anticyclonic circulation during winter than during summer (Fig. 6), as well as more anticyclonic circulation during certain years (not shown; see Fig. 8 and 10 in Mysak et al, 2005).

The simulated sea-ice area export is in good agreement with data; we find correlation coefficients of $r=0.73$ ($p<0.01$) between the simulation and the observed monthly Fram Strait sea-ice area flux of Vinje et al (1998) and Kwok and Rothrock (1999). The model also captures the reported change in the correlation between the winter sea-ice area export and the winter NAO index in the late 1970s (see Hilmer

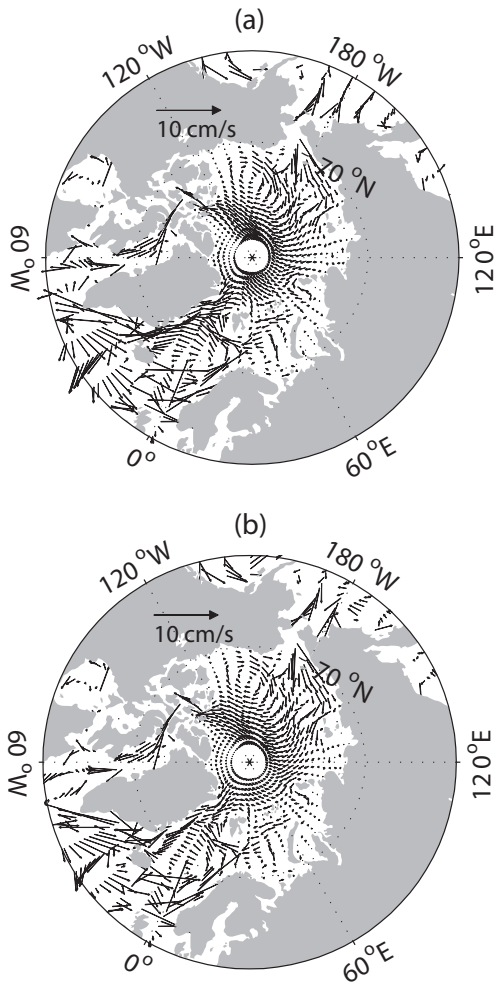


Fig. 6 Average simulated (a) winter (DJF) and (b) summer (JJA) ocean velocity field in the top 108 m.

and Jung, 2000), with a significant positive correlation after 1977/78 ($r=0.57$ for winter 1977/78–1996/97, $p<0.01$), and no significant correlation before 1977. However, the simulated sea-ice volume export is smaller than observed by a factor of three, due to the smaller than observed sea-ice thickness in the model.

The simulated volume fluxes through Bering Strait (1.2 Sv) and the CAA (1.5 Sv) are close to observations, but the volume inflow from the GIN seas into the Arctic Ocean is smaller than observed. We find a simulated volume inflow of 1.6 Sv through Fram Strait and 0.8 Sv through the Barents Sea, compared to observational estimates of 9–10 Sv (Schauer et al, 2004; Fahrbach et al, 2001) and 2.2 Sv (Blindheim, 1989; Ingvaldsen et al, 2004; Dickson et al, 2007), respectively. This also leads to smaller than observed outflow from the Arctic Ocean, so that overall the Arctic Ocean is more isolated from the North Atlantic in the model than in reality.

Many of the model biases that we find in our simulation are not unique to the UVic ESCM, but occur in many current generation regional and global models. The range of the simulated FW content, for example, differs widely between the regional models participating in AOMIP (Steiner et al, 2004), as well as between ten global climate models included in the IPCC report (Holland et al, 2007). A too deep and too thick Atlantic Layer, as well as a missing cold halocline, are also a common feature among AOMIP models (Holloway et al, 2007) and global climate models (Holland et al, 2007). In addition, different model types also have specific problems. For example, Proshutinsky et al (2007) found that the Beaufort Gyre weakened over the course of the simulation in 3D regional coupled sea ice-ocean models that were not restored to salinity, while models that use a strong restoring show limited variability (Gerdes et al, 2008). Due to their generally lower resolution, global models tend to underestimate the northward heat transport into the Arctic Ocean, which often leads to an unrealistic sea-ice edge and larger than observed FW exports through the Barents Sea (Holland et al, 2007). Similar to regional ocean-ice models, global ocean-ice models also need to use salinity restoring to close their hydrological balance (Griffies et al, 2009). Fully coupled global climate models on the other hand do not need to use restoring, but they can not be used for hindcast experiments because their variability is model generated. Intermediate complexity models like the UVic ESCM can be used for hindcasts because they are forced with reanalysis winds, and have the advantage that they do not use salinity or temperature restoring. This makes the UVic ESCM a worthwhile tool to investigate the variability of the Arctic Ocean FW budget during the last decades, despite the biases in the simulation of the Arctic climate.

4 Simulated Arctic Ocean FW budget

4.1 Climatological mean FW budget

The simulated climatological Arctic Ocean FW budget, averaged over the 58 years of the experiment (1950–2007), is shown in Table 1, together with the FW budgets derived from observation (Aagaard and Carmack, 1989; Serreze et al, 2006). In agreement with Aagaard and Carmack (1989) and Serreze et al (2006), the largest FW source in the model is the (prescribed) river discharge into the Arctic Ocean, followed by the Bering Strait inflow, and the net precipitation over the Arctic Ocean. The largest FW sink in the model is the liquid FW export through the CAA, followed by solid and liquid FW exports through Fram Strait, liquid and solid FW exports through the Barents Sea, and solid FW export through the CAA.

The simulated FW exports through Fram Strait and the CAA are biased low compared to Serreze et al (2006), due

Table 1 Climatological present-day Arctic Ocean freshwater (FW) budget based on the UVic ESCM simulation (averaged over 1950–2007) and on observations (Aagaard and Carmack, 1989; Serreze et al, 2006). All FW fluxes are calculated relative to a reference salinity of 34.8, and are given in km^3/year . They are net annual mean fluxes through a channel, combining negative and positive fluxes through a strait, where applicable. All oceanic fluxes are calculated over the full depth of the ocean boundaries. Positive values indicate FW sources, and negative values indicate FW sinks for the Arctic Ocean. Note that the river runoff was prescribed in the simulation.

FW fluxes	UVic ESCM	Aagaard & Carmack	Serreze et al.
River runoff	2762	3300	3200
P-E	981	900	2000
Bering Strait liquid FW	1545	1670	2500
CAA liquid FW	-2040	-920	-3200
Fram Strait liquid FW	-880	-980	-2660
Barents Sea liquid FW	-874	-290	-90
Bering Strait solid FW	-1	-	-
CAA solid FW	-107	-	-160
Fram Strait solid FW	-921	-2790	-2300
Barents Sea solid FW	-457	-	-
Net	8	890	-710

to smaller than observed FW source terms, too thin sea-ice, and much larger than observed Barents Sea FW exports in the simulation. The smaller FW input is due to too low simulated precipitation in high latitudes, which leads to a too high salinity of the Pacific water inflow through Bering Strait (mean salinity of 33.4 instead of 32.5) and a low bias in the net precipitation over the Arctic Ocean. The solid and liquid FW exports through the Barents Sea are larger than observed due to the sea-ice edge position (which is too far south) and its effect on local ocean currents. However, the total liquid FW export into the GIN seas, through both Fram Strait and the Barents Sea, is in better agreement with observations (see Table 1). Compared to other model FW budgets (Steele et al, 1996; Zhang and Zhang, 2001; Miller and Russell, 2000; Haak et al, 2005; Holland et al, 2006, 2007; Köberle and Gerdes, 2007; Arzel et al, 2008), the FW fluxes in our simulation tend to be lower. A direct comparison of simulated FW flux terms with other model studies is, however, difficult, as some have a closed CAA and/or Bering Strait, some use salinity restoring, and some use much higher prescribed river runoff.

4.2 Variability of FW fluxes

The simulated climatological (58-year mean) Arctic Ocean FW budget nearly closes, with the total FW import and export essentially balancing each other (see the bottom line in Table 1). This is not the case on shorter timescales, due to the interannual variability of the individual FW fluxes. In some years, the total FW import is larger than the export, which leads to an accumulation of FW in the Arctic, while in

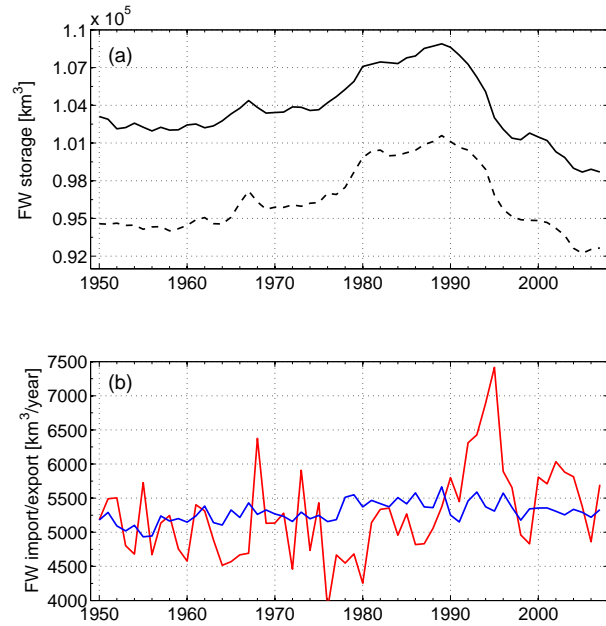


Fig. 7 (a) Simulated total (liquid plus solid FW, shown as *solid line*) and liquid (shown as *dashed line*) Arctic Ocean FW storage in the top 518 m. (b) Simulated annual mean Arctic Ocean FW import (*blue line*) and export (*red line*). The reference salinity used to calculate FW storage and fluxes is 34.8.

other years the opposite is true (see Fig. 7). We find that the variability of the simulated FW export is much larger than the variability of the FW import (see Fig. 7b), in general agreement with observations (Serreze et al, 2006) and modeling results (e.g., Holland et al, 2006; Köberle and Gerdes, 2007). The largest simulated variability of the FW export terms is seen in the liquid FW export through the CAA, followed by the liquid Fram Strait FW export, the solid Fram Strait export, and the liquid and solid Barents Sea FW exports (see Fig. 8a and Table 2). The simulated liquid FW export shows the largest variability on multi-year to decadal timescales, whereas the solid FW export exhibits more variability on annual timescales (see Fig. 8a). This is in agreement with model results from Köberle and Gerdes (2003, 2007).

The liquid FW exports through the CAA, Fram Strait, and Barents Sea are not correlated with each other, although all of them show large FW exports in the 1990s, leading to the largest simulated export of liquid (and total) FW from the Arctic Ocean during the study period (see Fig. 8a). The simulated liquid FW export through the CAA shows a shift from generally lower values before 1982, to generally higher values after 1982, with a local maximum in 1985 and the overall largest export in 1990 (see Fig. 8a). The liquid FW export through Fram Strait shows three periods of increased export, between 1952–1959, 1967–1977, and 1993–2002. Periods with increased Barents Sea liquid FW export are

Table 2 Mean and standard deviation (std) of all simulated FW fluxes [km^3/year]. For the ocean fluxes, the liquid FW fluxes are given first, followed by the solid FW fluxes.

	CAA	Fram Strait	Barents Sea	Bering Strait	P-E	River Runoff
mean	-2040/-107	-880/-921	-874/-457	1545/1	981	2762
std	461/47	259/229	229/182	143/2	61	0

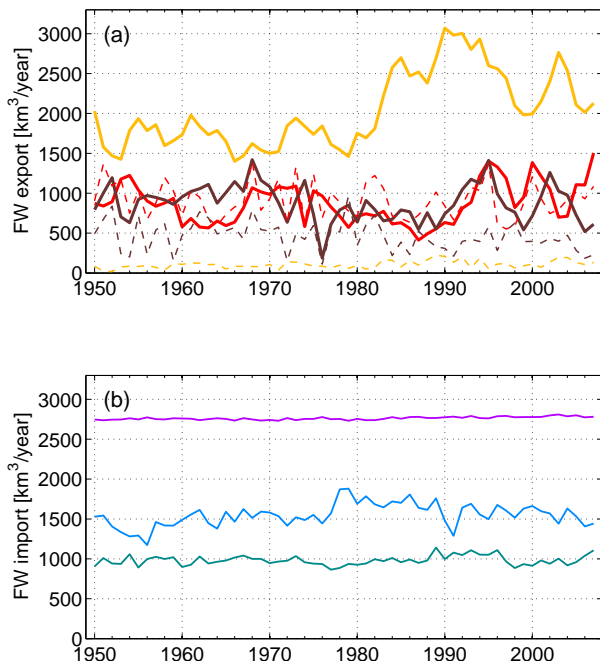


Fig. 8 (a) Simulated annual mean net FW export through the CAA (orange), the Fram Strait (red), and the Barents Sea (brown). All exports are shown as positive values. Liquid FW exports are shown as solid lines, and solid FW exports as dashed lines. (b) Simulated annual mean net FW imports through the Bering Strait (light blue), river runoff (purple), and net precipitation (turquoise).

1951–1952, 1961–1963, 1965–1970, 1992–1996, and 2002–2003.

Due to the lack of long-term observations of either the volume or the FW flux through the CAA or Fram Strait (see Dickson et al, 2007, for a summary of currently available data), we can not directly validate the variability of the simulated liquid FW fluxes through the CAA and Fram Strait. A comparison with other available model results shows that certain features occur in different models, but the details of the export variability are model dependent. Among the robust features is the period of increased liquid FW export through the CAA between 1982 and 1999, which is also seen in the simulation of Köberle and Gerdes (2007). The liquid Fram Strait FW export maxima in the 1990s, with a peak in 1995, is also seen in model simulations of Karcher et al (2005) and Köberle and Gerdes (2007). It is also supported by observational data, which show lower than average salinities in the East Greenland Current in the early to mid 1990s (Blindheim et al, 2000). Finally, the increased liquid FW ex-

port through Fram Strait in the late 1960s and early to mid 1970s is also simulated by all three models, but its duration and magnitude vary. In agreement with the results presented here, Karcher et al (2005) show a smaller liquid FW export maximum in the 1970s than in the 1990s, whereas Köberle and Gerdes (2007) find the largest liquid FW export in the 1970s, corresponding to the very large FW storage decrease in their simulation during this time (see discussion in section 4.3).

Regarding the variability of the FW source terms, we find that the simulated Bering Strait inflow shows much larger variability than the net precipitation over the Arctic Ocean (see Fig. 8b and Table 2), in agreement with observations (Serreze et al, 2006). The largest signal in the simulated Bering Strait FW inflow is associated with a shift towards higher FW input between 1977 and 1989 (see Fig. 8b), mainly due to increased transports through the strait. The timing of this increase in the flow corresponds to the observed regime shift in the atmospheric circulation over the Pacific Ocean between 1976–1988 (e.g., Trenberth, 1990; Trenberth and Hurrell, 1994). The regime shift is accompanied in the model by a rise in the rigid-lid pressure in the northern North Pacific south of Bering Strait. This in turn leads to an increase in the rigid-lid pressure gradient (equivalent to a sea surface height (SSH) gradient in the real ocean) between the North Pacific and the Arctic Ocean, driving the increase in the transport through Bering Strait. Because SSH gradients are equivalent to rigid-lid pressure gradients in their dynamical effect on the ocean (see Pacanowski, 1995, for details), we will from now on refer only to SSH gradients in our analysis. Between 1977 and 1989, the mean northward Bering Strait FW transport is $255 \text{ km}^3/\text{year}$ higher than before 1977, which adds up to an additional import of 3315 km^3 of FW. This increase in the Bering Strait FW influx contributes about as much to the FW accumulation in the Arctic Ocean during the 1980s as the reduced FW export through Fram Strait or Barents Sea. Hence, a fixed Bering Strait inflow, as used in many regional models, would lead to a smaller simulated FW accumulation during the 1980s than found here.

4.3 Variability of the Arctic Ocean FW content

The simulated FW content in the upper 518 m of the Arctic Ocean shows two maxima, a small one in the late 1960s, and a large one in the 1980s (see Fig. 7a). Overall, the Arctic

Ocean is more saline at the end of the simulation than at the beginning, after a fresher episode in the 1980s (see Fig. 7a). This salinification of the Arctic Ocean over the period 1950–2007 agrees with the trend towards saltier water in the central Arctic Ocean found by Polyakov et al (2008) for the 20th century in observational data. The periods of increased FW content in the 1960s, early 1980s, and early 1990s found in their study are also in general agreement with the maxima found here, but the relative magnitude and the exact timing differs. Note that the number of observations are limited before 1970, and the data have large error bars.

Compared to other model simulations by Häkkinen and Proshutinsky (2004) and Köberle and Gerdes (2007), the times of liquid FW storage maxima and minima occur within 1 or 2 years of the times found here (see Fig. 7a and their Fig. 2a and Fig. 4b, respectively). This points to a robust feature in the ice-ocean system, despite differences in the model domain and the simulated sea-ice conditions. However, the amplitude of these changes varies from model to model. The largest liquid FW content maximum occurs in the late 1980s in this study and in the one of Häkkinen and Proshutinsky (2004), but in 1968–1970 in the study of Köberle and Gerdes (2007). In the latter simulation, the maximum of 1989 is only the third largest maximum (after that of 1968–1970 and 1982). In addition to these differences, the liquid FW storage in the simulation of Köberle and Gerdes (2007) also shows a much larger amplitude than found here or in Häkkinen and Proshutinsky (2004), especially during the 1960s and 1970s. This shows that the relative magnitude of the 1960s versus the 1980s FW maximum is model dependent, whereas the times of the major FW storage maxima and minima are a robust feature across different models. Recent observational results of Proshutinsky et al (2009) suggest that the conditions in the Beaufort Gyre during the 1990s differed significantly from previous decades, with larger FW storage in the Beaufort Gyre and a contracted and south-eastward shifted center of the FW content maximum. Given that the majority of the Arctic FW is stored in the Beaufort Gyre, this suggests that the FW content maximum in the 1990s was larger than the one in the late 1960s, but more data is needed to confirm this.

4.4 Sensitivity to initial conditions and CAA channel configuration

To test the sensitivity of the simulation to its initial conditions, five additional simulations for the 1948–2005 period were performed. The initial conditions were derived from spin-up simulations which were forced by the same orbital and CO₂ forcing, but with different wind forcing. These experiments show noticeable differences until the early 1960s, with the largest differences in the first 2 years (1948–1949;

see Fig. 9a). Results up until the early 1960s should therefore be treated with caution, and results for the first 2 years are excluded from the analysis. We conclude that the smaller FW accumulation during the 1960s compared to the 1980s is a robust feature of our simulation, and not the result of initial conditions.

To investigate the sensitivity of our results to the choice of the CAA channel configuration, we performed additional simulations for two different channel locations (see Fig. 10b–c), as well as for different channel cross-sections (and hence different magnitudes of the FW export), and for a closed CAA. The winds used to derive the initial conditions for these additional experiments were the same as for the control run. We find that in the simulation with the CAA closed, the amplitude of the FW storage maximum in 1967 is smaller and the amplitude of the maximum in 1989 is larger than in simulations with an opened CAA (see Fig. 9b, c). Consistent with this behavior, the amplitude of the simulated FW storage maximum in 1967 increases when the mean CAA liquid FW export increases, while the amplitude of the FW storage maximum in 1989 decreases with increasing mean CAA FW exports (see Fig. 9c). This means that differences in the simulated CAA FW export have some influence on the amplitude of the FW storage maxima in 1967 and 1989. However, for all liquid CAA FW fluxes in the sensitivity experiments we performed (which reach from 684 km³/year to 2564 km³/year), the FW maximum in 1989 is always the dominant one.

As shown in Fig. 9b–c, the effect of different CAA locations (with the same mean liquid CAA FW export) on the variability of the Arctic FW storage is smaller than the effect of changes in the liquid CAA FW export through changes in the cross-section area. In general, changes in the liquid FW export through the CAA due to changes in the location or the cross-sectional area mainly affect the magnitude of the liquid FW export through Fram Strait, but do not lead to large changes in the temporal variability of the liquid FW export through Barents Sea or Fram Strait (not shown).

5 Mechanisms for the liquid FW export variability

5.1 Influence of salinity and volume flux anomalies on the liquid FW export

To test whether the simulated variability of the liquid FW export is driven mainly by upper ocean salinity or volume flux anomalies, we split the liquid FW export into a time-mean component and three time-varying terms. We only consider the upper 330 m of the water column, which is the maximum depth of the CAA and the layer where 92% of the Fram Strait liquid FW export takes place in the model. The

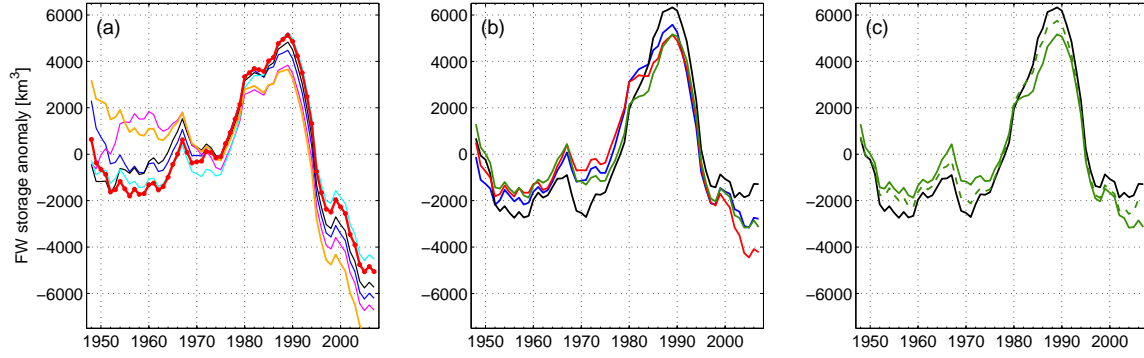


Fig. 9 (a) FW storage anomalies for simulations with different initial conditions. The simulation analyzed in this paper is shown as a *thick red line*. (b) FW storage anomalies for simulations with a closed CAA (*black*) and with the CAA opened in three different configurations (*red, blue, and green*, which correspond to the CAA locations shown in Fig 10a, b, and c, respectively). The three simulations with the CAA opened all have the same mean CAA liquid FW export of about 1600 km^3 . (c) FW storage anomalies for simulations with a closed CAA (*black*) and with an open CAA (*green*). The simulations with an open CAA have the same geographic location of the CAA, but different mean liquid CAA FW exports due to differences in the cross-sectional area (larger mean export ($-1595 \text{ km}^3/\text{year}$) shown as *solid line*, smaller mean export ($-685 \text{ km}^3/\text{year}$) as *dashed line*). Similar results are found for the other two CAA locations (not shown).

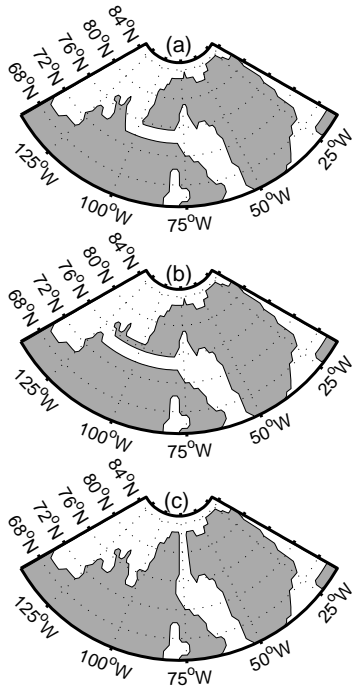


Fig. 10 Land-ocean masks for the three different CAA channel locations used in the CAA sensitivity experiments shown in Fig. 9b–c. Configuration (a) is the mask used for results presented in other sections.

liquid FW flux through a strait (F_{FW}) is calculated as

$$F_{FW} = \int_A v_{\perp} \frac{S_{ref} - s}{S_{ref}} dA = \int_A v_{\perp} S dA, \quad (1)$$

where v_{\perp} is the velocity component perpendicular to the strait, S_{ref} is the reference salinity, s is the salinity at the strait, $S = (S_{ref} - s)/S_{ref}$ is the normalized salinity anomaly, and A is the area of the cross-section of the

strait perpendicular to the flow. Splitting up S and v_{\perp} into time-mean ($\langle S \rangle$ and $\langle v_{\perp} \rangle$) and time-varying parts (S' and v'_{\perp}), and using an overbar to denote the spatial integral over the cross-sectional area of the strait, we can write the liquid FW transport through a strait from equation (1) as

$$F_{FW} = \overline{\langle S \rangle \langle v_{\perp} \rangle} + \overline{v'_{\perp} \langle S \rangle} + \overline{S' \langle v_{\perp} \rangle} + \overline{S' v'_{\perp}}. \quad (2)$$

In this equation, $\overline{\langle S \rangle \langle v_{\perp} \rangle}$ is the mean FW flux through a strait, $\overline{v'_{\perp} \langle S \rangle}$ is the FW flux due to the advection of the mean salinity by the volume flux anomaly, $\overline{S' \langle v_{\perp} \rangle}$ is the FW transport associated with the advection of salinity anomalies by the mean flow, and $\overline{S' v'_{\perp}}$ is the FW flux due to the advection of salinity anomalies by the anomalous volume flow.

As shown in Fig. 11, the variability of the liquid FW export is mainly controlled by changes in the volume flux ($\overline{v'_{\perp} \langle S \rangle}$), but changes in the salinity of the outflow ($\overline{S' \langle v_{\perp} \rangle}$) are also important at certain times. The volume flux driven liquid FW export anomalies show a correlation of $r=0.97$ and $r=0.95$ with the total liquid FW export in the CAA and Fram Strait, respectively. The correlation of the salinity driven liquid FW export anomaly with the total liquid FW export is lower but still significant, with $r=0.71$ for the CAA and $r=0.53$ for Fram Strait ($p < 0.01$). The correlation of $\overline{v'_{\perp} \langle S \rangle}$ with $\overline{S' \langle v_{\perp} \rangle}$ is larger in the CAA than in Fram Strait ($r=0.52$ and $r=0.34$ with $p < 0.01$, respectively). This shows that in the CAA, the volume and salinity driven liquid FW export anomalies are more strongly coupled than in Fram Strait.

The volume flux driven liquid FW export anomaly in the CAA increases in the early 1980s, with a maximum in 1990 (Fig. 11a). The salinity driven CAA liquid FW export anomaly ($\overline{S' \langle v_{\perp} \rangle}$) peaks in the mid 1990s, and generally increases between the mid 1960s and the mid 1990s, followed by a decrease after the mid 1990s (Fig. 11a). In Fram Strait,

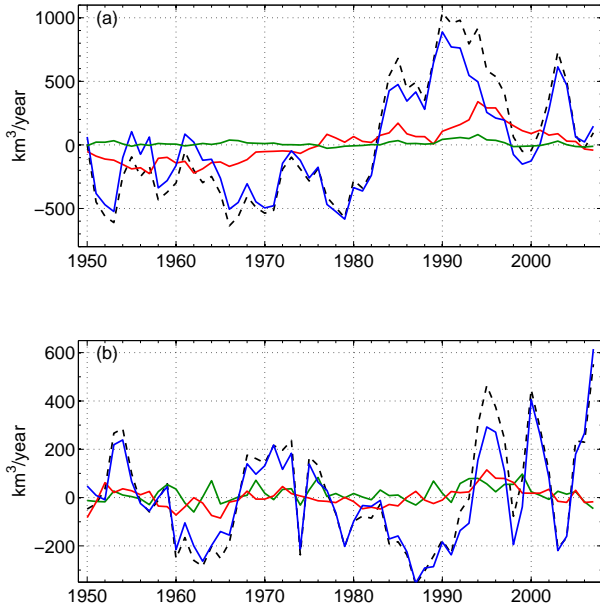


Fig. 11 Annual liquid FW export anomalies (black dashed line) for the (a) CAA and (b) Fram Strait (top 330 m only). In blue, the advection of the mean salinity by the volume flux anomaly ($\overline{v_{\perp} \langle S \rangle}$); in red, the advection of salinity anomalies by the mean flow ($\overline{S' \langle v_{\perp} \rangle}$); in green, the advection of the salinity anomaly by the volume flux anomaly ($\overline{S' v_{\perp}}$). Positive values show an increased FW export compared to the mean.

the volume flux driven liquid FW export shows three periods of increased export, with the largest anomalies during the last decade (Fig. 11b). The salinity anomalies in Fram Strait are generally in phase with the low-frequency variability of the volume export, and contribute most to the liquid Fram Strait FW export during the large export event of the 1990s (Fig. 11b). This export of fresher water through Fram Strait in the early to mid 1990s is supported by data of Blindheim et al (2000), as well as by model results of Karcher et al (2005). However, model results of Köberle and Gerdes (2007) show no significant changes in the salinity of the Fram Strait outflow during this time.

5.2 Local Forcing of the liquid FW export

In order to assess what is driving the liquid FW export variability, we constructed indices for the SSH difference and the local wind field for the CAA and Fram Strait. For the CAA, the SSH difference was calculated as difference between the mean values in the Beaufort Sea and Baffin Bay (see blue boxes in Fig. 1). The local wind used in this analysis is the east-west component in a 300 km wide region along the CAA channel. For Fram Strait, the SSH difference was calculated as the difference between the mean values in regions north and south of Fram Strait (see the blue boxes in Fig. 1). The local wind field used for Fram Strait is the north-south component in a 300 km fetch centered around

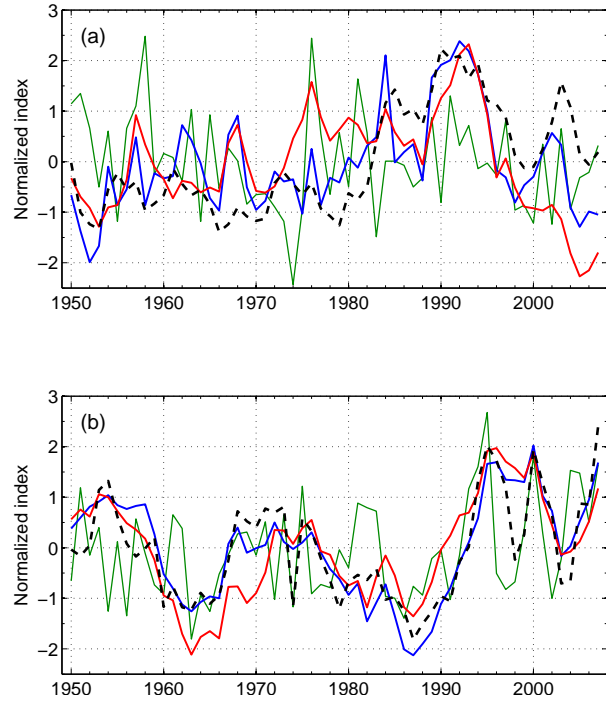


Fig. 12 The liquid (a) CAA and (b) Fram Strait FW export (black dashed lines), together with the local wind forcing multiplied by -1 (green lines) for the (a) CAA and (b) Fram Strait, and the SSH difference (blue lines) between (a) Beaufort Sea and Baffin Bay and (b) between a region up to 700 km north and south of Fram Strait (see Fig. 1 for the regions used). The red lines in (a) and (b) show the SSH difference diagnosed from changes in the salinity in the regions used to calculate the SSH difference (halosteric SSH change). All time series show annual mean values, normalized by the standard deviation.

the latitude of Fram Strait (which is shown as red line in Fig. 1).

The liquid FW export through the CAA, as well as the volume flux driven liquid FW export anomaly ($\overline{v_{\perp} \langle S \rangle}$), are well correlated with the SSH difference between the Beaufort Sea and Baffin Bay ($r=0.68$ for both, $p<0.01$) (see Fig. 12a). The control of the volume flux variability in the CAA by the SSH difference between the Beaufort Sea and Baffin Bay is in agreement with model results of Kliem and Greenberg (2003) and Newton et al (2008), as well as with the data study of Prinsenberg and Bennett (1987). We find that the simulated SSH difference is mainly controlled by SSH changes in the Beaufort Sea, rather than by SSH changes in Baffin Bay ($r^2=0.50$ and $r^2=0.14$, respectively, not shown). As shown in Fig. 12a, a large part (52%) of the SSH changes in the Beaufort Sea, and hence also of the SSH difference, is caused by salinity changes (the so-called halosteric SSH change, see Steele and Ermold, 2007). The salinity driven liquid CAA FW export anomaly ($\overline{S' \langle v_{\perp} \rangle}$) is therefore also correlated with the SSH in the Beaufort Sea ($r=0.85$ at a lag of 1 year, $p<0.01$) and the SSH difference across the CAA ($r=0.62$ at a lag of 2 years, $p<0.01$).

Due to this high correlation with the SSH in the Beaufort Sea, volume and salinity driven CAA liquid FW export anomalies also show a high cross-correlation ($r=0.52$, $p<0.01$). In contrast, the local along-strait wind forcing is found to have no significant correlation with the simulated CAA FW export or the volume and salinity driven liquid FW export anomalies (see Fig. 12a). This might be due to the largely landfast ice in the CAA channel, which insulates the ocean from the wind forcing.

The annual north-south SSH difference across Fram Strait is highly correlated with the liquid FW export through Fram Strait ($r=0.86$, $p<0.01$, see Fig. 12b), as well as with the volume flux driven liquid FW export anomaly ($r=0.77$, $p<0.01$) and the salinity driven liquid FW export anomaly ($r=0.54$, $p<0.01$). A calculation of the halosteric SSH change shows that the halosteric SSH change on average explains the majority ($r^2=0.72$) of the changes in the SSH difference (see the red line in Fig. 12b). Only in the late 1960s does the halosteric SSH difference change not explain most of the SSH difference variability, which is due to a freshening in the region south of Fram Strait between 1962 and 1972 (not shown). Except for the late 1960s, changes in the region north of Fram Strait dominate the SSH difference variability (not shown). The local wind field is also significantly correlated with the liquid FW export ($r=0.50$, $p<0.01$) (see Fig. 12b). The local wind only affects the volume flux driven liquid FW export anomaly ($r=0.51$, $p<0.01$), not the salinity driven liquid FW export anomaly (no significant correlation).

5.3 Large-scale forcing of the liquid FW export

As can be seen in Fig. 13a–b, the FW storage in the Beaufort Sea is shifted towards the North American coast during times of increased liquid FW export through the CAA compared to times of lower liquid CAA FW export. This is due to a cyclonic circulation anomaly in the Beaufort Gyre during times of increased liquid CAA FW export (not shown), which in turn is caused by a change in the large-scale atmospheric forcing over the Arctic Ocean. Figure 14 shows that the AO index and the CAA liquid FW export have a similar variability, and over the period 1950 to 2007, the peak in the cross-correlation between the AO index and the liquid CAA FW export occurs at a lag of 1 year ($r=0.54$, $p<0.01$). The maximum correlation coefficient increases to $r=0.71$ and $r=0.75$ ($p<0.01$) at a 1-year lag for the 3- and 5-year running means, respectively, which suggests that the variability of the liquid FW export is influenced mainly by the lower-frequency variability of the atmospheric forcing. Composites of winter SLP 1 year before large and small liquid CAA FW exports show that the Icelandic Low is much deeper and the Arctic High is weaker before large liquid FW exports (see Fig. 13a, b). These SLP patterns are consistent

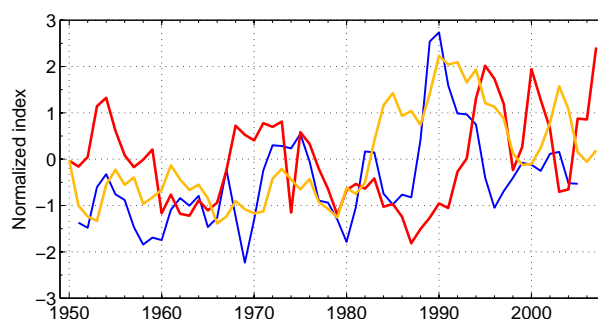


Fig. 14 The Arctic Oscillation (AO) index from NOAA/NCEP (blue) compared to the simulated liquid FW export through the CAA (orange) and Fram Strait (red). The time series are 3-year running means of the annual mean values, normalized by the standard deviation.

with the typical SLP patterns seen during positive and negative AO/NAO phases. In the Beaufort Sea, the weaker Arctic High leads to a cyclonic circulation anomaly (see also Proshutinsky et al, 2002), which releases FW from the central Beaufort Gyre and leads to the shift of the FW storage in the Beaufort Sea towards the North American coast seen in Fig. 13a–b.

Mainly through changes in the density, these changes in the FW distribution are responsible for the SSH changes in the Beaufort Sea, which were found to drive the variability of the volume export through the CAA (see section 5.2). In addition, these changes provide more low salinity water for the export through the CAA. The SSH in the Beaufort Sea shows a significant cross-correlation with the AO index at a lag of 1 year ($r=0.58$ for the annual mean and $r=0.78$ for the 3-year running mean; $p<0.01$). Both volume flux anomalies and salinity anomalies contribute to the high correlation of the CAA liquid FW export with the AO index, with $r=0.69$ at a 1-year lag and $r=0.68$ ($p<0.01$) at a 4-year lag for the 3-year running means, respectively.

During years of large liquid Fram Strait FW export, the FW storage along the northern Greenland and North American coast is increased (Fig. 13c–d) compared to years of low liquid FW export. While this pattern of FW storage changes is similar as for the CAA liquid FW export, the peak in the cross-correlation between the annual mean and the 3-year running mean AO index and the liquid FW export through Fram Strait occurs at a lag of 6 years ($r=0.35$ and $r=0.45$, $p<0.01$). An examination of the composite of the winter SLP over the Arctic 6 years before increased liquid Fram Strait FW exports shows the typical pattern for NAO positive winters, with a very strong Icelandic Low and decreased pressure over the central Arctic. As explained earlier, this leads to a release of FW from the Beaufort Gyre due to a cyclonic circulation anomaly, which increases the FW storage along the northern coast of Greenland, increasing the SSH north of Fram Strait and supplying fresher water for the export. The mean lag between the AO index and the liquid FW

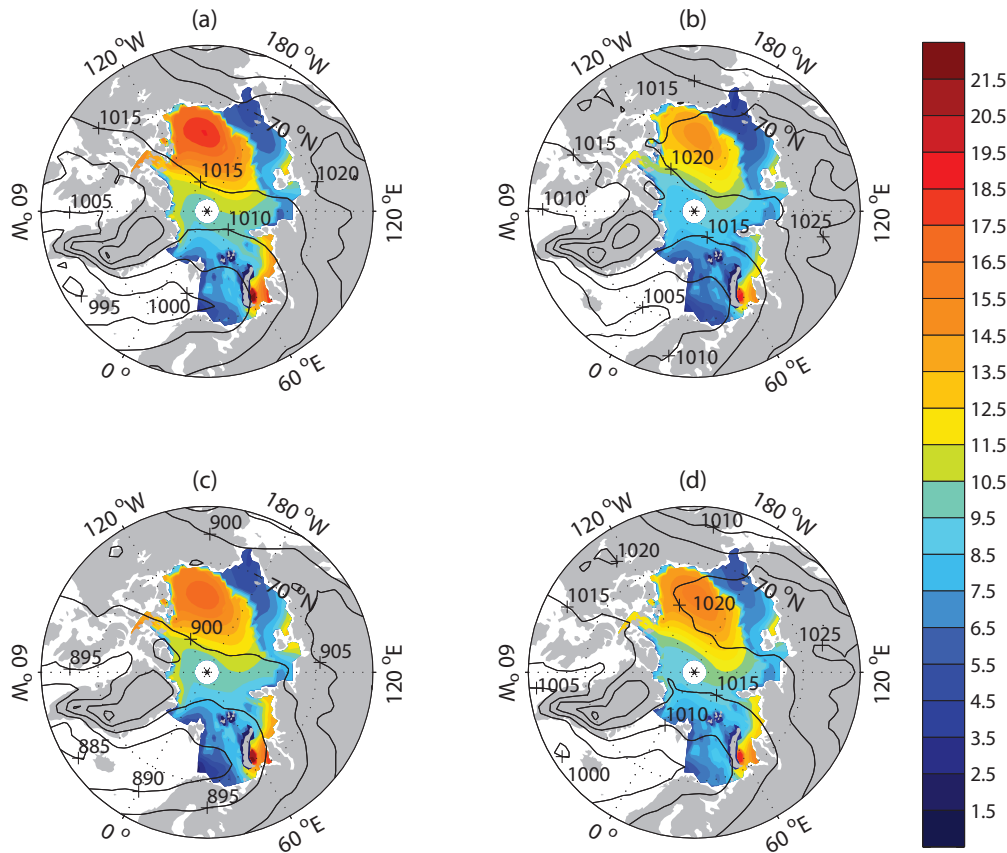


Fig. 13 Composites of the FW storage in the Arctic Ocean, expressed as column of FW [m], during times of increased (a, c) and decreased (b, d) liquid FW export through the CAA (a-b) and Fram Strait (c-d). The composites are formed from years that show a FW export larger/smaller than one standard deviation. Composites of the winter NCEP sea level pressure (SLP) field [hPa, 5 hPa spacing] 1 (a-b) and 6 (c-d) years prior to the years of large/small FW export are also shown (*black lines*), to illustrate the typical pressure pattern over the Arctic that leads to these export events.

export is larger than for the CAA, due to the longer travel time from the Beaufort Gyre region to the Fram Strait than to the CAA.

Both the volume driven liquid Fram Strait FW export anomaly and the salinity driven Fram Strait liquid FW export anomaly also show high correlations with the 3-year running mean AO index ($r=0.45$ at a lag of 6 years and $r=0.62$ at a lag of 5 years, respectively; $p<0.01$), which shows the importance of the large-scale atmospheric circulation for both anomalies. However, other effects like the local wind forcing also play a role for the volume driven liquid Fram Strait FW export anomaly, decreasing the correlation with the indices for the large-scale atmospheric circulation compared to the CAA (i.e., $r=0.45$ versus $r=0.69$; $p<0.01$).

5.4 Differences between large liquid FW export events

The lag between the Fram Strait liquid FW export and the AO index is smaller during the liquid FW export maximum

in the late 1960s to mid 1970s, and larger for the maximum during the 1990s, whereas the lag between the CAA liquid FW export and the AO is constant in time (see Fig. 14). We find that this change in the lag of the Fram Strait liquid FW export is due to different FW source regions for these export events. During the late 1960s to mid 1970s, most of the liquid FW exported through Fram Strait came from the Eurasian basin, whereas during the 1990s a large part came from the Canadian Basin (see Fig. 15). The differences in the location of the FW source regions for the Fram Strait liquid FW export are associated with changes in the strength and position of the Beaufort Gyre and the associated FW distribution in the Arctic Ocean (see Fig. 16), as well as the existence of a local Eurasian ocean circulation cell between 1960 and 1967 that disappears afterwards (not shown).

The simulated circulation changes in the Arctic Ocean that lead to the increased export of liquid FW from the Canadian Basin through Fram Strait during the early to mid 1990s are in agreement with results of Tucker et al (2001) and Pfirman et al (2004), which are based on data from

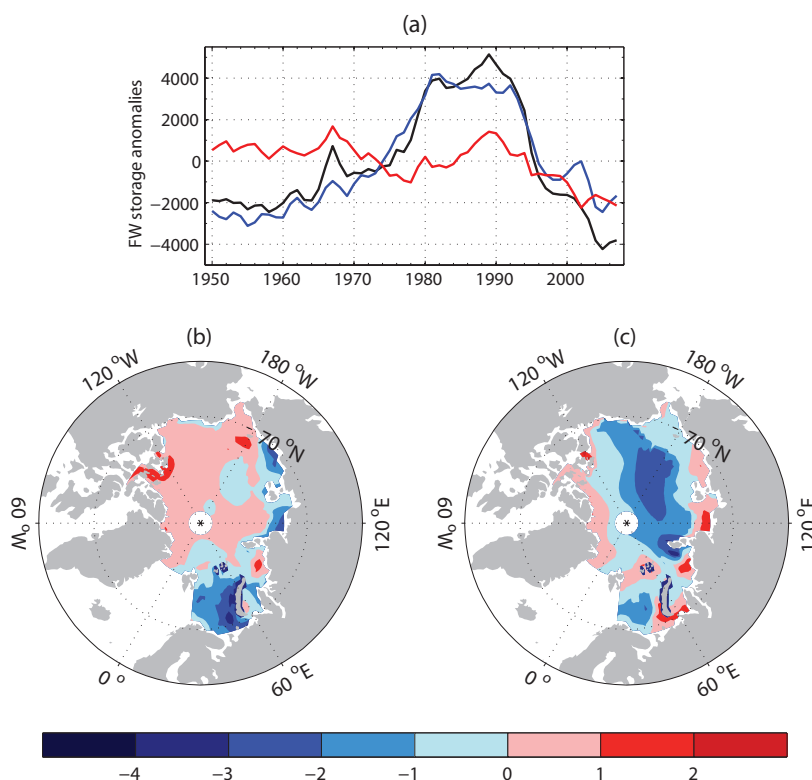


Fig. 15 (a) Liquid FW storage anomalies [km^3] in the upper 518 m, for the full Arctic Ocean (*black*), the Canadian basin (*blue*), and the Eurasian basin (*red*). The border that separates the Canadian and the Eurasian basin is the Lomonosov ridge. (b–c) Changes in the liquid FW storage, expressed as column of FW [m] in the top 518 m relative to a salinity of 34.8, between (b) 1968 and 1975 and (c) 1990 and 1997. This shows the regions of FW release during the two maximum periods of increased liquid FW export through Fram Strait.

the International Arctic Buoy Program. They found that the main source regions of the Fram Strait sea-ice export changed from the Kara and Laptev seas to the East-Siberian and Chukchi seas in the late 1980s in response to changes in the atmospheric forcing, which led to the export of large amounts of thick multiyear ice that was previously recirculating in the Beaufort Gyre. While the response of sea-ice export and liquid FW to changes in the atmospheric forcing is different, they are both strongly influenced by large-scale atmospheric circulation changes. Unfortunately, the simulated changes in the source regions of liquid FW during the late 1960s and early 1970 can not be compared to data from the International Arctic Buoy Program, as it only began in 1979.

5.5 Summary: Proposed mechanism of liquid FW export variability

We conclude that the variability of the large-scale atmospheric circulation controls the variability of the liquid FW export from the Arctic through its effect on the strength of the Beaufort Gyre, which controls the FW distribution and the SSH field in the Arctic Ocean. This agrees with

the hypothesis of Proshutinsky et al (2002), as well as with recent observational evidence presented by Proshutinsky et al (2009). We find that changes in the Arctic SSH field in turn affect the CAA and Fram Strait volume exports through changes in the SSH difference across these straits. Changes in the FW distribution also affect the salinity of the CAA and Fram Strait outflows, but this effect is found to be less important than the volume flux changes. The CAA liquid FW export responds to changes in the AO index with a lag of 1 year, whereas the Fram Strait liquid FW export responds with a mean lag of 6 years. The lag between the CAA liquid FW export and the AO index is constant, whereas the lag between the Fram Strait liquid FW export and the AO index is not. The lag of the Fram Strait liquid FW export depends on the location of the FW source for the increased FW export, which in turn depends on differences in the SLP field over the Arctic Ocean. Due to this difference in the lag, as well as the different travel times of salinity anomalies from the Beaufort Sea to the CAA and Fram Strait, the Fram Strait and CAA liquid FW exports are not in phase. The influence of the local wind forcing in the Fram Strait area further modulates the variability of the Fram Strait liquid FW export, in contrast

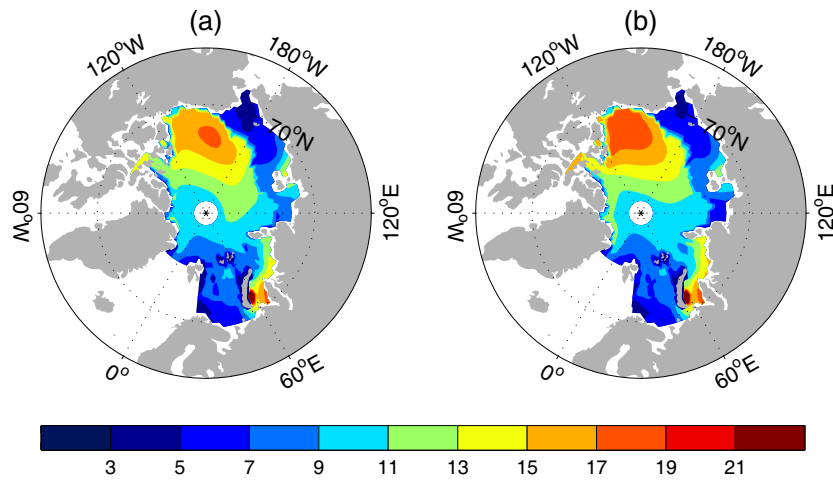


Fig. 16 Average liquid FW storage, expressed as column of FW [m], for (a) 1968–1975 and (b) 1990–1997, the two periods of large liquid Fram Strait FW exports.

to the CAA, where the local wind has no effect on the variability of the liquid FW export.

6 Influence of the liquid FW export on the oceanic heat flux and the Atlantic MOC

6.1 Oceanic heat flux

We find that the mean simulated net ocean heat flux from the GIN seas to the Arctic Ocean between 1950–2007 is 13.9 TW, calculated relative to the simulated mean sea surface temperature in Fram Strait ($T_{Ref} = -1.7^\circ\text{C}$). Most of this heat is entering the Arctic Ocean through Fram Strait (10.9 TW), with only a smaller amount entering through the Barents Sea (3.0 TW). Observational studies, using the observed mean surface water temperature in Fram Strait (-0.01°C) as reference temperature (Aagaard and Greisman, 1975), also show a larger heat flux through Fram Strait than through Barents Sea (e.g., Aagaard and Greisman, 1975; Rudels, 1987; Simonsen and Haugan, 1996). However, the simulated ocean heat transport into the Arctic Ocean is smaller when compared to recent observational estimates of 16–40 TW for the net Fram Strait ocean heat flux (Schauer et al, 2004). Given that the temperature difference between the reference temperatures (-1.7°C in the model and -0.01°C in observations) and the temperature of the incoming Atlantic water (0.5°C in the model and $2\text{--}3^\circ\text{C}$ in observations by Schauer et al, 2004) is similar in the model and in observations, we conclude that the discrepancy in the simulated Fram Strait heat flux is mainly due to the low bias in the simulated volume flow from the North Atlantic into the Arctic Ocean.

In the simulation, 78% of the ocean heat flux into the Arctic Ocean passes through Fram Strait (see Fig. 17). The

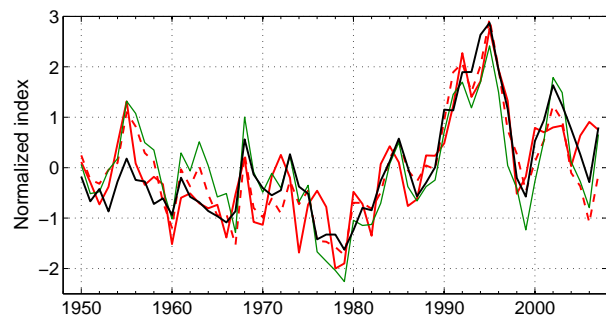


Fig. 17 Annual mean Normalized index (normalized by the standard deviation) of the total simulated net ocean heat flux from the North Atlantic to the Arctic Ocean (*solid red line*), the net ocean heat flux through Fram Strait alone (*red dashed line*), the total liquid FW export from the Arctic (*black*), and the Atlantic water inflow through Fram Strait (*green*; taken as the northward volume flow through Fram Strait below 330 m).

Fram Strait heat flux is also the source of 71% of the variance of the total net ocean heat transport into the Arctic. We find that 85% of the simulated variance of the Fram Strait ocean heat flux into the Arctic Ocean is due to changes in the volume inflow of Atlantic water (see Fig. 17), with temperature changes of the inflowing water being much less important (not shown). The total liquid FW export from the Arctic Ocean (through the CAA, Fram Strait, and the Barents Sea combined) is highly correlated with the Fram Strait Atlantic water inflow, the Fram Strait heat transport, and the total heat transport into the Arctic Ocean ($r=0.85$, $r=0.86$, and $r=0.89$, respectively, $p < 0.05$) (see Fig. 17). Note however that the total Atlantic heat flux into the Arctic Ocean only shows a correlation of $r=0.45$ ($p < 0.05$) with the total volume export (rather than the total FW export) from the Arctic. This shows that the link between Arctic liquid FW export and oceanic heat import is not only due to the mass

conservation in the model. The mechanisms that leads to this link between the FW export and the heat import are the topic of future work.

Given that climate simulations for the 21st century show an increase in the liquid FW export from the Arctic (e.g., Haak et al, 2005; Holland et al, 2006, 2007; Koenigk et al, 2007), our results suggest that this could be associated with an increased oceanic heat flux into the Arctic Ocean in the future. Whether this increased oceanic heat import can affect the Arctic sea-ice cover is unclear, as it depends on how much of this Atlantic heat can reach the mixed layer, which is a topic still under debate. Yang et al (2001, 2004) argue that mixing associated with strong storms can reach below the halocline, leading to the entrainment of Atlantic heat into the mixed layer. Regions where an increase in the vertical heat flux to the surface due to storm induced mixing has been observed are the Fram Strait area (Yang et al, 2004), the Beaufort Sea (Yang et al, 2001), and the region north of Svalbard (Steele and Morison, 1993). Timmermans et al (2008) on the other hand argue that away from boundary regions, the vertical heat flux from the Atlantic water to the mixed layer is small, and occurs mainly through double-diffusion. More research on the vertical heat flux from the Atlantic water to the Arctic mixed later is necessary to determine the possible effect of an increased Atlantic heat transport into the Arctic on the sea-ice cover.

6.2 Atlantic MOC

The mean simulated maximum overturning streamfunction in the North Atlantic is 15.9 Sv, with a standard deviation of 1.0 Sv. This compares well with the observed estimate of 15 ± 2 Sv given by Ganachaud and Wunsch (2000). In the model, deep water is formed mainly in the Irminger Sea, with a secondary maximum in the Norwegian Sea (see the black boxes in Fig. 18a). In contrast to observations, no deep water is formed in the Labrador Sea. In the following, we use the mean depth of the convective adjustment, referred to as convection depth from now on, as well as the mean surface salinity in the Irminger and Norwegian seas to investigate the effect of the FW export from the Arctic on the surface salinity, the convection depth, and the MOC strength.

In the 1950–2007 period, the largest drop in the simulated MOC strength occurs a few years after the large FW export event in the late 1960s to mid 1970s (see Fig. 19a). Smaller reductions in the MOC strength occur in the mid 1950s and mid 1990s, again following increased FW export from the Arctic. In all cases, these reductions in the MOC strength are preceded by a decrease in the surface salinity and the convection depth in the deep water formation regions of the North Atlantic about 5 to 6 years earlier, with much larger changes observed in the Irminger Sea than in

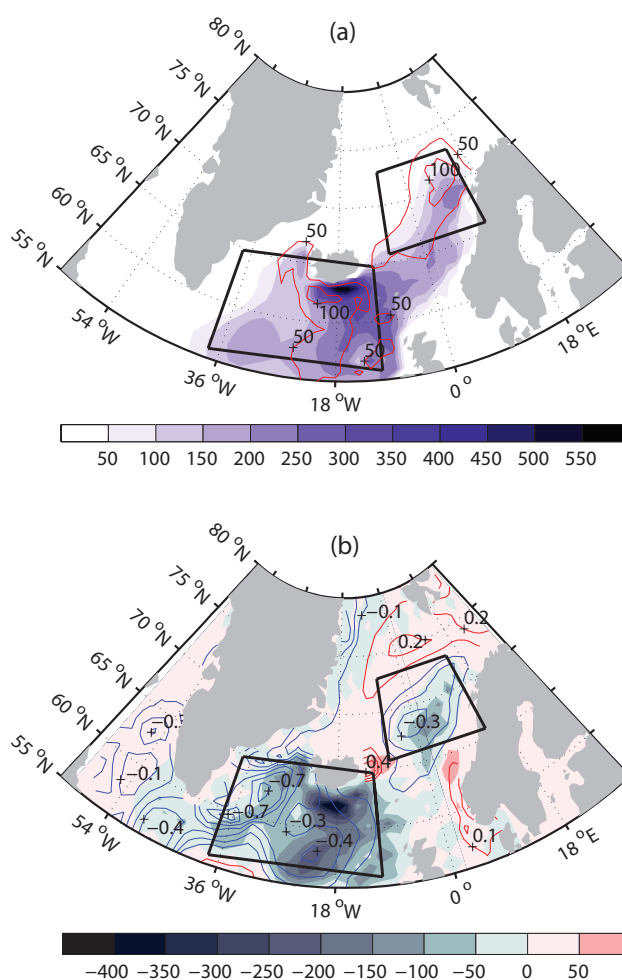


Fig. 18 (a) Mean simulated depth of convective adjustment (*shaded*, in meters) and the standard deviation of the depth of convective adjustment (*red contours*; line spacing is 50 m). (b) Change in the convection depth between 1967 and 1972 (*shaded*; in meters) and the associated salinity change in the top 50 meters (*lines*; *blue* shows a freshening; *red* a salinification; line spacing is 0.1). The *black boxes* show the regions over which the average deep convection and salinity for the Irminger and Norwegian seas is calculated. The exact choice of the size of the boxes does not influence the results, as long as the main centers of deep convection are included. We show the changes between 1967 and 1972, which is the period when the largest changes in the simulated convection depth occur (see Fig. 19b). Very similar patterns are found for changes between 1951 and 1953 and between 1993 and 1996, but with smaller amplitudes.

the Norwegian Sea (see Fig. 18b and Fig. 19b). The correlation between the 3-year running means of the surface salinity (top 50 m) and the convection depth in the Irminger and Norwegian seas are $r=0.79$ and $r=0.94$ ($p<0.05$), respectively, while the correlation between the MOC strength and the 3-year running mean convection depth is significant for lags between 4 and 8 years, and reaches a maximum for a 5-year lag ($r=0.49$ for both regions, $p<0.05$). The changes in the surface salinity in the deep convection regions are in turn caused by changes in the FW export through Fram Strait

and Barents Sea (called FW export into the GIN seas in the following). In the Irminger Sea, the correlation is highest between the 3-year running mean surface salinity and the total (solid and liquid) FW export into the GIN seas ($r=-0.51$ at a lag of 2 years, $p<0.05$). In the Norwegian Sea the correlation of the 3-year running mean surface salinity is highest with the liquid FW export into the GIN seas ($r=-0.40$ at zero-year lag, $p<0.05$). This difference between the two deep water formation regions is due to the fact that sea-ice export from the Arctic predominantly melts in the Irminger Sea, rather than in the deep convection region of the Norwegian Sea. The liquid FW export through the CAA shows no correlation with the salinity anomalies or the convection depth in both deep water formation regions of the model.

The correlation of the 3-year running mean FW export with the MOC strength has a maximum correlation of $r=-0.45$ at a 1-year lag for the liquid FW export into the GIN seas, and $r=-0.37$ for the total FW export into the GIN seas ($p<0.05$). This means that 20% of the variance of the MOC strength is explained by the variability of the FW export from the Arctic into the GIN seas, whereas the FW export into the Labrador Sea has no effect on the simulated MOC strength. However, in models where deep water formation is also present in the Labrador Sea, the CAA FW export might have a larger effect. The MOC strength also shows a significant correlation with the total heat flux into the Arctic Ocean at a lag of 12 years (the time scale for the surface ocean circulation in the North Atlantic - results not shown). This explains approximately 15% of the variance of the ocean heat flux into the Arctic Ocean.

When the CAA is closed, the simulated MOC strength is reduced (from 15.9 Sv to 14.5 Sv), but shows a very similar variability than when the CAA is opened (see Fig. 19a). This agrees with results of Komuro and Hasumi (2005), who found a reduction in the MOC strength when the CAA was closed because of a freshening of the Fram Strait outflow. This change in the salinity of the Fram Strait outflow had a larger effect on the MOC strength than the missing FW export into the Labrador Sea when the CAA was closed. In our simulation, the mean salinity of the FW outflow through Fram Strait is also lower when the CAA is closed compared to when it is opened (33.49 versus 33.80).

The impact of the liquid FW export on the MOC is especially important for the future because climate models predict an increase in the liquid FW export during the 21st century (e.g., Holland et al, 2006, 2007; Koenigk et al, 2007). However, whether the Fram Strait or CAA liquid FW export will increase more strongly during the 21st century appears to be model dependent. While the CCSM3 shows a much stronger increase of the liquid FW export through Fram Strait than through the CAA during the 21st century (Holland et al, 2006), the increase is about equally large for both straits in the ECHAM5/MPI-OM (Koenigk et al,

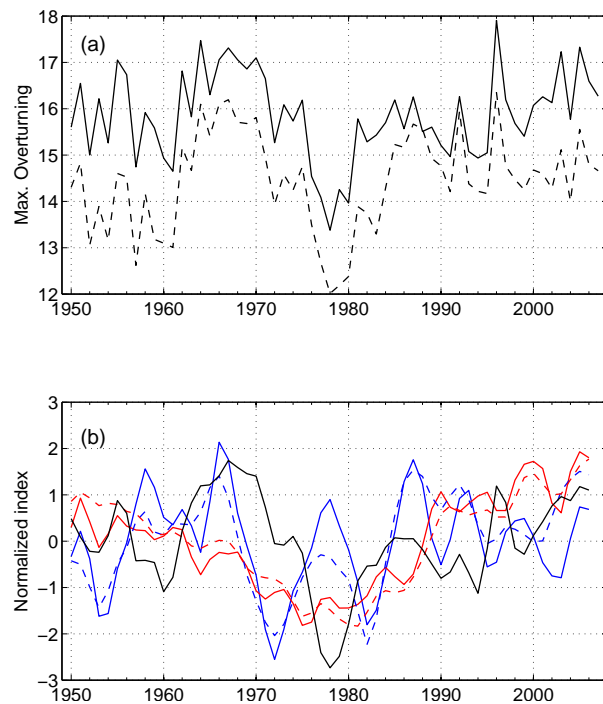


Fig. 19 (a) The maximum strength of the annual mean Atlantic MOC [in Sv] for simulations with the CAA opened (*solid*) and the CAA closed (*dashed*). (b) 3-year running mean normalized index of the depth of convective adjustment (*solid line*) and surface salinity (*dashed line*) in the deep water formation region in the Irminger Sea (*blue*) and in the Norwegian Sea (*red*) (shown as boxes in Fig. 18), compared to the 3-year running mean normalized index of the MOC strength (*black*).

2007). The potential effects of these future changes in the Arctic liquid FW export on the MOC strength remain to be assessed.

7 Conclusions

In this study we investigated the mechanisms driving the variability of the liquid FW export from the Arctic Ocean. We used a 1.8° by 0.9° resolution version of the global energy and mass conserving UVic ESCM, forced with daily NCEP winds, to perform a simulation for the period 1950–2007. Besides the river runoff, for which a climatological cycle was prescribed, all Arctic FW fluxes were simulated by the model.

We showed that the simulated variability of the liquid FW export is mainly controlled by the variability of the large-scale atmospheric circulation over the Arctic. Changes in the cyclonicity of the large-scale atmospheric forcing cause changes between cyclonic and anticyclonic circulation regimes in the Arctic Ocean, which lead to changes in the Arctic Ocean FW distribution due to Ekman transport. These changes in the FW distribution lead to changes in

the SSH difference across the CAA and Fram Strait, which drive the variability of the volume export, as well as to changes in the salinity of the surface outflow through CAA and Fram Strait. The liquid FW export variability is found to be dominated by variations in the volume export. Salinity anomalies are generally less important, but have a larger contribution in the CAA than in Fram Strait. Both volume export changes and salinity anomalies in the outflow are associated with changes in the large-scale atmospheric circulation through its effect on the strength of the circulation in the Beaufort Gyre, which in turn controls the large-scale FW and SSH distribution. The resulting changes in the SSH difference across the CAA and Fram Strait are found to explain a large part of the variance of the liquid FW export (46% in the CAA, and 74% in Fram Strait). In Fram Strait, the local wind forcing also explains a significant part of the variance (25%) of the liquid FW export through its effect on the volume flux. In the CAA, the local wind forcing plays no significant role, possibly due to the presence of landfast ice.

The liquid FW export through the CAA is found to respond to changes in the AO index with a mean lag of 1 year, whereas the Fram Strait liquid FW export shows a mean lag of 6 years. In contrast to the liquid FW export through the CAA, the magnitude of the lag of the Fram Strait liquid FW export behind the AO index depends on differences in the source region for the Fram Strait FW export. These source regions in turn strongly depend on the position and strength of the Beaufort Gyre, as well as on the existence of a local ocean circulation cell in the Eurasian basin. Hence, while the AO index captures changes in the CAA liquid FW export very well, the relationship with the Fram Strait liquid FW export is less robust and more complicated, due to the influence of the local wind forcing and the effect of local circulation changes in the Eurasian basin.

All these results are robust to changes in the initial conditions, as well as to changes in the location and size of the CAA channel in the model. Certain features of the simulation (e.g., timing of FW storage maxima, increased liquid FW export through the CAA during the 1980s to the mid 1990s, increased liquid FW export through Fram Strait in the late 1960s to mid 1970s and in the mid 1990s) agree with results from regional sea ice-ocean models (Häkkinen and Proshutinsky, 2004; Karcher et al, 2005; Köberle and Gerdes, 2007). Other features, most importantly the amplitude of the FW storage anomalies as well as the relative importance of the two main FW storage maxima (late 1960s versus the late 1980s), differ between models. Our results indicate that differences in the magnitude of the simulated CAA FW export, as well as the use of a constant prescribed versus a variable simulated Bering Strait FW import, can explain some of these differences. A more detailed investigation of the physical reasons for these differences in the

model simulations it is an important next step in order to better understand the dynamics of the liquid FW export from the Arctic, but is beyond the scope of the present paper.

Results from this study also show that during times of increased liquid FW export from the Arctic, the oceanic heat transport into the Arctic Ocean is increased, due to an increase in the Atlantic water inflow. Increased liquid FW export from the Arctic Ocean is also found to reduce the simulated MOC strength in the North Atlantic, through its effect on the surface salinity in the deep water formation regions, which in turn affects the convection depth in these regions. In agreement with the study of Komuro and Hasumi (2005), we find that the liquid FW export into the GIN seas shows a larger impact on the MOC strength than the liquid FW export through the CAA.

Based on our results, a trend towards a more positive phase of the NAO/AO in the future, as suggested for example by Osborn (2004), Kuzmina et al (2005), and Serreze and Francis (2006), might lead to increased FW export from the Arctic Ocean to the northern North Atlantic. Model simulations for the 21st century show that the liquid FW export is indeed increasing, while the Arctic sea-ice export is decreasing (Holland et al, 2006). Our results suggest that this could be associated with an increase in the ocean heat flux into the Arctic Ocean. Whether such an increase in the heat flux could have an effect on the sea-ice cover of the Arctic Ocean is not clear, as the magnitude of the vertical heat flux from the Atlantic water to the Arctic mixed layer, as well as the processes that lead to it, are still under debate (e.g. Steele and Morison, 1993; Yang et al, 2001, 2004; Timmermans et al, 2008).

Acknowledgements We thank Michael Eby (University of Victoria) for making the high resolution version of the UVic ESCM available to us, as well as for technical assistance with the model. Advice from Andreas Schmittner (Oregon State University) on opening Bering Strait is much appreciated. We also thank Asa Rennermalm (University of California Los Angeles) for providing us with the code and data to use the climatological river runoff, as well as Rüdiger Gerdes (Alfred Wegener Institute for Polar and Marine Research) for useful discussions. The thoughtful comments of the anonymous reviewers are greatly appreciated, and helped us to improve the manuscript. NCEP reanalysis data was provided by NOAA/OAR/ESRL PSD, Boulder, Colorado, USA, from their Web site at <http://www.cdc.noaa.gov/>. This work was supported by a fellowship from the Studienstiftung des deutschen Volkes awarded to A. Jahn; a NSERC Discovery Grant, a NSF Office of Polar Program Grant (OPP-0230325), and an Arctic Science Program Grant (ARC-0520496) awarded to B. Tremblay; and a NSERC Discovery Grant awarded to L. A. Mysak.

References

Aagaard K, Carmack EC (1989) The role of sea ice and other fresh water in the Arctic circulation. *J Geophys Res* 94(C10):14,485–14,498, DOI 10.1029/JC094iC10p14485

- Aagaard K, Greisman P (1975) Toward new mass and heat budgets for the Arctic Ocean. *J Geophys Res* 80:3821–3827, DOI 10.1029/JC080i027p03821
- Aagaard K, Swift JH, Carmack EC (1985) Thermohaline circulation in the Arctic Mediterranean seas. *J Geophys Res* 90(C7):4833–4846, DOI 10.1029/JC090iC03p04833
- Arfeuille G, Mysak LA, Tremblay LB (2000) Simulation of the interannual variability of the wind-driven Arctic sea-ice cover during 1958–1998. *Clim Dyn* 16(2–3):107–121, DOI 10.1007/PL00013732
- Arzel O, Fichefet T, Goosse H, Dufresne JL (2008) Causes and impacts of changes in the Arctic freshwater budget during the twentieth and twenty-first centuries in an AOGCM. *Clim Dyn* 30(1):37–58, DOI 10.1007/s00382-007-0258-5
- Berger A (1978) Long-term variations of daily insolation and quaternary climatic changes. *J Atmos Sci* 35:2362–2367, DOI 10.1175/1520-0469(1978)035<2362:LTVODI>2.0.CO;2
- Bitz CM, Holland MM, Weaver AJ, Eby M (2001) Simulating the ice-thickness distribution in a coupled climate model. *J Geophys Res* 106(C2):2441–2464, DOI 10.1029/1999JC000113
- Bitz CM, Gent PG, Woodgate RA, Holland MM, Lindsay R (2006) The influence of sea ice on ocean heat uptake in response to increasing CO₂. *J Climate* 19(11):2437–2450, DOI 10.1175/JCLI3756.1
- Blindheim J (1989) Cascading of Barents Sea bottom water into the Norwegian Sea. *Rapp PV Réun Cons Int Explor Mer* 188:49–58
- Blindheim J, Borovkov V, Hansen B, Malmberg SA, Turrell WR, Østerhus S (2000) Upper layer cooling and freshening in the Norwegian Sea in relation to atmospheric forcing. *Deep Sea Res* 47(4):655–680, DOI 10.1016/S0967-0637(99)00070-9
- Dickson R, Rudels B, Dye S, Karcher M, Meincke J, Yashayaev I (2007) Current estimates of freshwater flux through Arctic and subarctic seas. *Prog Oceanogr* 73(3–4):210–230, DOI 10.1016/j.pocean.2006.12.003
- Dickson RR, Meincke J, Malmberg SA, Lee AJ (1988) The “Great Salinity Anomaly” in the northern North Atlantic 1968–1982. *Prog Oceanogr* 20(2):103–151, DOI 10.1016/0079-6611(88)90049-3
- Dickson RR, Osborn TJ, Hurrell JW, Meincke J, Blindheim J, Adlandsvik B, Vinje T, Alekseev G, Maslowski W (2000) The Arctic Ocean response to the North Atlantic Oscillation. *J Climate* 13(15):2671–2696, DOI 10.1175/1520-0442(2000)013<2671:TAORTT>2.0.CO;2
- Fahrbach E, Meincke J, Østerhus S, Rohardt G, Schauer U, Tverberg V, Verduin J (2001) Direct measurements of volume transports through Fram Strait. *Polar Res* 20(2):217–224, DOI 10.1111/j.1751-8369.2001.tb00059.x
- Fanning AG, Weaver AJ (1996) An atmospheric energy-moisture model: Climatology, interpentadal climate change and coupling to an ocean general circulation model. *J Geophys Res* 101:15,111–15,128, DOI 10.1029/96JD01017
- Ganachaud A, Wunsch C (2000) Improved estimates of global ocean circulation, heat transport and mixing from hydrographic data. *Nature* 408:453–457, DOI 10.1038/35044048
- Gent PR, McWilliams JC (1990) Isopycnal mixing in ocean circulation models. *J Phys Oceanogr* 20(1):150–155, DOI 10.1175/1520-0485(1990)020<0150:IMIOCM>2.0.CO;2
- Gerdes R, Köberle C (2007) Comparison of Arctic sea ice thickness variability in IPCC Climate of the 20th Century experiments and in ocean-sea ice hindcasts. *J Geophys Res* 112, DOI 10.1029/2006JC003616
- Gerdes R, Karcher M, Köberle C, Fieg K (2008) Chapter 17: Simulating the long-term variability of liquid freshwater export from the Arctic Ocean. *Arctic-Subarctic Ocean Fluxes*, Eds R R Dickson and J Meincke and P Rhines, Springer Science and Business Media B V pp 405–425
- Gregory JM, Saenko OA, Weaver AJ (2003) The role of the Atlantic freshwater balance in the hysteresis of the meridional overturning circulation. *Clim Dyn* 21(7–8):707–717, DOI 10.1007/s00382-003-0359-8
- Griffies SM, Biastoch A, Böning C, Bryan F, Danabasoglu G, Chassignet EP, England MH, Gerdes R, Haak H, Hallberg RW, Hazeleger W, Jungclaus J, Large WG, Madec G, Pirani A, Samuels BL, Scheinert M, Gupta AS, Severijns CA, Simmons HL, Treguier AM, Winton M, Yaeger S, Yin J (2009) Coordinated ocean-ice reference experiment (COREs). *Ocean Model* 26(1–2):1–46, DOI 10.1016/j.ocemod.2008.08.007
- Haak H, Jungclaus J, Koenigk T, Sein D, Mikolajewicz U (2005) Arctic Ocean freshwater budget variability. *Arctic Subarctic Ocean Fluxes (ASOF) Newslet* 3:6–8
- Häkkinen S (1995) Simulated interannual variability of the Greenland Sea Deep Water formation and its connection to surface forcing. *J Geophys Res* 100(C3):4761–4770, DOI 10.1029/94JC01900
- Häkkinen S, Mellor GL (1992) Modeling the seasonal variability of a coupled Arctic ice-ocean system. *J Geophys Res* 97:20,285–20,304, DOI 10.1029/92JC02037
- Häkkinen S, Proshutinsky A (2004) Freshwater content variability in the Arctic Ocean. *J Geophys Res* 109, DOI 10.1029/2003JC001940
- Harder M, Lemke P, Hilmer M (1998) Simulation of sea ice transport through Fram Strait: Natural variability and sensitivity to forcing. *J Geophys Res* 103(C3):5595–5606, DOI 10.1029/97JC02472
- Hilmer M, Jung T (2000) Evidence for a recent change in the link between the North Atlantic Oscillation and Arctic

- sea ice export. *Geophys Res Lett* 27(7):989–992, DOI 10.1029/1999GL010944,
- Holland MM, Bitz CM, Eby M, Weaver AJ (2001) The role of ice-ocean interactions in the variability of the North Atlantic thermohaline circulation. *J Climate* 14(5):656–675, DOI 10.1175/1520-0442(2001)014;0656:TROIOL;2.0.CO;2
- Holland MM, Finnis J, Serreze MC (2006) Simulated Arctic Ocean freshwater budgets in the twentieth and twenty-first centuries. *J Climate* 19(23):6221–6242, DOI 10.1175/JCLI3967.1
- Holland MM, Finnis J, Barrett AP, Serreze MC (2007) Projected changes in Arctic Ocean freshwater budgets. *Geophys Res Lett* 112, DOI 10.1029/2006JG000354
- Holloway G, Dupont F, Golubeva E, Häkkinen S, Hunke E, Jin M, Karcher M, Kauker F, Maltrud M, Maqueda MAM, Maslowski W, Platov G, Stark D, Steele M, Suzuki T, Wang J, Zhang J (2007) Water properties and circulation in Arctic Ocean models. *J Geophys Res* 112, DOI 10.1029/2006JC003642
- Hunke EC, Dukowicz JK (1997) An elastic-viscous-plastic model for sea ice dynamics. *J Phys Oceanogr* 27(9):1849–1867, DOI 10.1175/1520-0485(1997)027;1849:AEVPMF;2.0.CO;2
- Hunkins K, Whitehead JA (1992) Laboratory simulation of exchange through Fram Strait. *J Geophys Res* 97(C7):11,299–11,321, DOI 10.1029/92JC00735
- Ingvaldsen RB, Asplin L, Loeng H (2004) The seasonal cycle in the Atlantic transport to the Barents Sea during the years 1997–2001. *Cont Shelf Res* 24:1015–1032, DOI 10.1016/j.csr.2004.02.011
- Kalnay E, Kanamitsu M, Kistler R, Collins W, Deaven D, Gandin L, Iredell M, Saha S, White G, Woollen J, Zhu Y, Leetmaa A, Reynolds R, Chelliah M, Ebisuzaki W, Higgins W, Janowiak J, Mo KC, Ropelewski C, Wang J, Jenne R, Joseph D (1996) The NCEP/NCAR 40-year reanalysis project. *Bull Amer Meteor Soc* 77(3):437–471, DOI 10.1175/1520-0477(1996)077;0437:TNYRP;2.0.CO;2
- Karcher M, Gerdes R, Kauker F, Köberle C, Yashayev I (2005) Arctic Ocean change heralds North Atlantic freshening. *Geophys Res Lett* 32, DOI 10.1029/2005GL023861
- Kauker F, Gerdes R, Karcher M, Köberle C, Lieser JL (2003) Variability of Arctic and North Atlantic sea ice: A combined analysis of model results and observations from 1978 to 2001. *J Geophys Res* 108(C6), DOI 10.1029/2002JC001573
- Keeling CD, Whorf TP (2005) Atmospheric CO₂ records from sites in the SIO air sampling network. In *Trends: A Compendium of Data on Global Change*. Carbon Dioxide Information Analysis Center, Oak Ridge National Laboratory, U.S. Department of Energy, Oak Ridge, Tenn., U.S.A.
- Kliem N, Greenberg DA (2003) Diagnostic simulations of the summer circulation in the Canadian Arctic Archipelago. *Atmos-Ocean* 41(4):273–289
- Köberle C, Gerdes R (2003) Mechanisms determining the variability of Arctic sea ice conditions and export. *J Climate* 16(17):2843–2858, DOI 10.1175/1520-0442(2003)016;2843:MDTVOA;2.0.CO;2
- Köberle C, Gerdes R (2007) Simulated variability of the Arctic Ocean freshwater balance 1948–2001. *J Phys Oceanogr* 37(6):1628–1644, DOI 10.1175/JPO3063.1
- Koenigk T, Mikolajewicz U, Haak H, Jungclaus J (2007) Arctic freshwater export in the 20th and 21st centuries. *J Geophys Res* 112, DOI 10.1029/2006JG000274
- Komuro Y, Hasumi H (2005) Intensification of the Atlantic deep circulation by the Canadian Archipelago throughflow. *J Phys Oceanogr* 35(5):775–789, DOI 10.1175/JPO2709.1
- Kuzmina SI, Bengtsson L, Johannessen OM, Drange H, Bobylev LP, Miles MW (2005) The North Atlantic Oscillation and greenhouse-gas forcing. *Geophys Res Lett* 32, DOI 10.1029/2004GL021064
- Kwok R, Rothrock DA (1999) Variability of Fram Strait ice flux and North Atlantic Oscillation. *J Geophys Res* 104(C3):5177–5190, DOI 10.1029/1998JC900103
- Lammers RB, Shiklomanov AI, Vörösmarty CJ, Fekete BM, Peterson BJ (2001) Assessment of contemporary Arctic river runoff based on observational discharge records. *J Geophys Res* 106(D4):3321–3334, DOI 10.1029/2000JD900444
- Lohmann G, Gerdes R (1998) Sea ice effects on the sensitivity of the thermohaline circulation. *J Climate* 11(11):2789–2803, DOI 10.1175/1520-0442(1998)011;2789:SIEOTS;2.0.CO;2
- Meredith M, Heywood K, Dennis P, Goldson L, White R, Fahrbach E, Schauer U, Østerhus S (2001) Freshwater fluxes through the western Fram Strait. *Geophys Res Lett* 28(8):1615–1618, DOI 10.1029/2000GL011992
- Miller JR, Russell GL (2000) Projected impact of climate change on the freshwater and salt budgets of the Arctic Ocean by a global climate model. *Geophys Res Lett* 27(8):1183–1186, DOI 10.1029/1999GL007001
- Mysak LA, Venegas SA (1998) Decadal climate oscillations in the Arctic: A new feedback loop for atmosphere-ice-ocean interactions. *Geophys Res Lett* 25(19):3607–3610, DOI 10.1029/98GL02782
- Mysak LA, Manak DK, Marsden RF (1990) Sea-ice anomalies observed in the Greenland and Labrador seas during 1901–1984 and their relation to an interdecadal Arctic climate cycle. *Clim Dyn* 5(2):111–133, DOI 10.1007/BF00207426
- Mysak LA, Wright KM, Sedláček J, Eby M (2005) Simulation of sea ice and ocean variability in the Arctic dur-

- ing 1955–2002 with an intermediate complexity model. *Atmos-Ocean* 43(1):101–118
- Newton B, Tremblay LB, Cane MA, Schlosser P (2006) A simple model of the Arctic Ocean response to annular atmospheric modes. *J Geophys Res* 111, DOI 10.1029/2004JC002622
- Newton R, Schlosser P, Martinson D, Maslowski W (2008) Freshwater distribution in the Arctic Ocean: simulation with a high-resolution model and model-data comparison. *J Geophys Res* 113, DOI 10.1029/2007JC004111
- Osborn TJ (2004) Simulating the winter North Atlantic Oscillation: the roles of internal variability and greenhouse gas forcing. *Clim Dyn* 22:605–623, DOI 10.1007/s00382-004-0405-1
- Pacanowski R (1995) MOM 2 documentation, user's guide, and reference manual. GFDL Ocean Group Technical Report, NOAA, Princeton
- Pfirman S, Haxby WF, Colony R, Rigor I (2004) Variability in the Arctic sea ice drift. *Geophys Res Lett* 31, DOI 10.1029/2004GL020063
- Polyakov IV, Alexeev VA, Belchansky GI, Dmitrenko IA, Ivanov VV, Kirillov SA, Korablev AA, Steele M, Timokhov LA, Yashayaev I (2008) Arctic Ocean freshwater changes over the past 100 years and their causes. *J Climate* 21:364–384, DOI 10.1175/2007JCLI1748.1
- Prange M, Gerdes R (2006) The role of surface freshwater flux boundary conditions in Arctic Ocean modelling. *Ocean Model* 13(1):25–43, DOI 10.1016/j.ocemod.2005.09.003
- Prinsenbergt SJ, Bennett EB (1987) Mixing and transport in Barrow Strait, the central part of the Northwest Passage. *Cont Shelf Res* 7(8):913–935, DOI 10.1016/0278-4343(87)90006-9
- Prinsenbergt SJ, Hamilton J (2005) Monitoring the volume, freshwater and heat fluxes passing through Lancaster Sound in the Canadian Arctic Archipelago. *Atmos-Ocean* 43(1):1–22
- Proshutinsky A, Bourke RH, McLaughlin FA (2002) The role of the Beaufort Gyre in Arctic climate variability: Seasonal to decadal climate scales. *Geophys Res Lett* 29(23), DOI 10.1029/2002GL015847
- Proshutinsky A, Ashik I, Häkkinen S, Hunke E, Krishfield R, Maltrud M, Maslowski W, Zhang J (2007) Sea level variability in the Arctic Ocean from AOMIP models. *J Geophys Res* 112, DOI 10.1029/2006JC003916
- Proshutinsky A, Krishfield R, Timmermans ML, Toole J, Carmack E, McLaughlin F, Zimmermann S, Itoh M, Shimada K (2009) The Beaufort Gyre fresh water reservoir: state and variability from observations. *J Geophys Res* accepted
- Proshutinsky AY, Johnson MA (1997) Two circulation regimes of the wind-driven Arctic Ocean. *J Geophys Res* 102(C6):12,493–12,514, DOI 10.1029/97JC00738
- Rennermalm AK, Wood EF, Déry SJ, Weaver AJ, Eby M (2006) Sensitivity of the thermohaline circulation to Arctic Ocean runoff. *Geophys Res Lett* 33, DOI 10.1029/2006GL026124
- Rennermalm AK, Wood EF, Weaver AJ, Eby M, Déry SJ (2007) Relative sensitivity of the Atlantic Meridional Overturning Circulation to river discharge into Hudson Bay and the Arctic Ocean. *J Geophys Res* 112, DOI 10.1029/2006JG000330
- Rudels B (1987) On the mass balance of the Polar Ocean with special emphasis on the Fram Strait. *Norsk Polar Skrifter* 188:1–53
- Saenko OA, Wiebe EC, Weaver AJ (2003) North Atlantic response to the above-normal export of sea ice from the Arctic. *J Geophys Res* 108(C7), DOI 10.1029/2001JC001166
- Saenko OA, Eby M, Weaver AJ (2004) The effect of sea-ice extent in the North Atlantic on the stability of the thermohaline circulation in global warming experiments. *Clim Dyn* 22(6–7):689–699, DOI 10.1007/s00382-004-0414-0
- Schauer U, Fahrbach E, Osterhus S, Rohardt G (2004) Arctic warming through the Fram Strait: Oceanic heat transport from 3 years of measurements. *J Geophys Res* 109, DOI 10.1029/2003JC001823
- Sedláček J, Mysak LA (2009) Sensitivity of sea ice to wind stress and radiative forcing since 1500: A model study of the Little Ice Age and beyond. *Clim Dyn* 32(6):817–831, DOI 10.1007/s00382-008-0406-6
- Sedláček J, Lemieux JF, Mysak LA, Tremblay LB, Holland DM (2007) The granular sea-ice model in spherical coordinates and its application to a global climate model. *J Climate* 20(24):5946–5961, DOI 10.1175/2007JCLI1664.1
- Serreze MC, Francis JA (2006) The Arctic amplification debate. *Climatic Change* 76(3–4):241–264, DOI 10.1007/s10584-005-9017-y
- Serreze MC, Barrett AP, Slater AG, Woodgate RA, Aagaard K, Lammers RB, Steele M, Moritz R, Meredith M, Lee CM (2006) The large-scale freshwater cycle of the Arctic. *J Geophys Res* 111, DOI 10.1029/2005JC003424
- Simonsen K, Haugan PM (1996) Heat budgets of the Arctic Mediterranean and sea surface heat flux parameterizations for the Nordic Seas. *J Geophys Res* 101(C3):6553–6576, DOI 10.1029/95JC03305
- Steele M, Ermold W (2007) Steric sea level change in the Northern Seas. *J Climate* 20(3):403–417, DOI 10.1175/JCLI4022.1
- Steele M, Morison JH (1993) Hydrography and vertical fluxes of heat and salt northwest of Svalbard in autumn. *J Geophys Res* 98(C6):10,013–10,024, DOI 10.1029/93JC00937
- Steele M, Thomas D, and S Martin DR (1996) A simple model study of the Arctic Ocean freshwater bal-

- ance. *J Geophys Res* 101(C9):20,833–20,848, DOI 10.1029/96JC01686
- Steele M, Morley R, Ermold W (2001) PHC: A global ocean hydrography with a high-quality Arctic Ocean. *J Climate* 14(9):2079–2087, DOI 10.1175/1520-0442(2001)014;2079:PAGOHW;2.0.CO;2
- Steiner N, Holloway G, Gerdes R, Häkkinen S, Holland D, Karcher M, Kauker F, Maslowski W, Proshutinsky A, Steele M, Zhang J (2004) Comparing modeled streamfunction, heat and freshwater content in the Arctic Ocean. *Ocean Model* 6:265–284, DOI 10.1016/S1463-5003(03)00013-1
- Timmermans ML, Toole J, Krishfield R, Winsor P (2008) Ice-Tethered Profiler observations of the double-diffusive staircase in the Canada Basin thermocline. *J Geophys Res* 113, DOI 10.1029/2008JC004829
- Tremblay LB (2001) Can we consider the Arctic Oscillation independently from the Barents Oscillation? *Geophys Res Lett* 28(22):4227–4230, DOI 10.1029/2000GL013740
- Trenberth KE (1990) Recent observed interdecadal climate changes in the Northern Hemisphere. *Bull Amer Meteor Soc* 71(7):988–993, DOI 10.1175/1520-0477(1990)071;0988:ROICCI;2.0.CO;2
- Trenberth KE, Hurrell JW (1994) Decadal atmosphere-ocean variations in the Pacific. *Clim Dyn* 9(6):303–319, DOI 10.1007/s003820050027
- Tucker WB, Weatherly JW, Eppler DT, Farmer LD, Bentley DL (2001) Evidence for rapid thinning of sea ice in the western Arctic Ocean at the end of the 1980's. *Geophys Res Lett* 28:2851–2854, DOI 10.1029/2001GL012967
- Vinje T (2001) Fram Strait ice fluxes and atmospheric circulation: 1950–2000. *J Climate* 14(16):3508–3517, DOI 10.1175/1520-0442(2001)014;3508:FSIFAA;2.0.CO;2
- Vinje T, Nordlund N, Kvambekk Å (1998) Monitoring ice thickness in Fram Strait. *J Geophys Res* 103(C5):10,437–10,449, DOI 10.1029/97JC03360
- Weaver AJ, Eby M (1997) On the numerical implementation of advection schemes for use in conjunction with various mixing parameterizations in the GFDL ocean model. *J Phys Oceanogr* 27(2):369–377, DOI 10.1175/1520-0485(1997)027;0369:OTNIOA;2.0.CO;2
- Weaver AJ, Marotzke J, Cummins PF, Sarachik E (1993) Stability and variability of the thermohaline circulation. *J Phys Oceanogr* 23(1):39–60, DOI 10.1175/1520-0485(1993)023;0039:SAVOTT;2.0.CO;2
- Weaver AJ, Eby M, Wiebe EC, Bitz CM, Duffy PB, Ewen TL, Fanning AF, Holland MM, MacFayden A, Matthews HD, Meissner KJ, Saenko O, Schmittner A, Wang H, Yoshimori M (2001) The UVic Earth System Climate Model: model description, climatology and application to past, present and future climates. *Atmos-Ocean* 39(4):361–428
- Woodgate RA, Aagaard K (2005) Revising the Bering Strait freshwater flux into the Arctic Ocean. *Geophys Res Lett* 32, DOI 10.1029/2004GL021747
- Yang J, Comiso J, Krishfield R, Honjo S (2001) Synoptic storms and the development of the 1997 warming and freshening event in the Beaufort Sea. *J Geophys Res* 28(5):799–802, DOI 10.1029/2000GL011896
- Yang J, Camiso J, Walsh D, Krishfield R, Honjo S (2004) Storm-driven mixing and potential impact on the Arctic Ocean. *J Geophys Res* 109, DOI 10.1029/2001JC001248
- Zhang J, Hibler WD, Steele M, Rothrock DA (1998) Arctic ice-ocean modeling with and without climate restoring. *J Phys Oceanogr* 28:191–217, DOI 10.1175/1520-0485(1998)028;0191:AIOMWA;2.0.CO;2
- Zhang X, Zhang J (2001) Heat and freshwater budgets and pathways in the Arctic Mediterranean in a coupled ocean/sea-ice model. *J Oceanogr Soc Japan* 57:207–234
- Zhang X, Ikeda M, Walsh J (2003) Arctic sea ice and freshwater changes driven by the atmospheric leading mode in a coupled sea ice-ocean model. *J Climate* 16(13):2159–2177, DOI 10.1175/2758.1